Paleoceanography and Paleoclimatology

RESEARCH ARTICLE
10.1029/2020PA004115

Key Points:

- Combined clumped isotope and Mg/Ca measurements validate previously published Mg/Ca-based studies from the Plio-Pleistocene Indo-Pacific
- No substantial cooling of the mixed layer in the Western Pacific Warm Pool during the last ~5 Myrs while the subsurface cooled from 4 Ma on
- Only a minor correction for Mg/Ca_{sw} changes is needed for the last ~5 Myrs

Supporting Information:

Supporting Information may be found in the online version of this article.

Correspondence to:

N. Meinicke,
nmeinicke@marum.de

Citation:

Meinicke, N., Reimi, M. A., Ravelo, A. C., & Meckler, A. N. (2021). Coupled Mg/Ca and clumped isotope measurements indicate lack of substantial mixed layer cooling in the Western Pacific Warm Pool during the last ~5 million years. *Paleoceanography and Paleoclimatology*, *36*, e2020PA004115. https://doi.org/10.1029/2020PA004115

Received 6 SEP 2020
Accepted 13 JUL 2021

Coupled Mg/Ca and Clumped Isotope Measurements Indicate Lack of Substantial Mixed Layer Cooling in the Western Pacific Warm Pool During the Last ~5 Million Years

N. Meinicke[1], M. A. Reimi[2], A. C. Ravelo[2], and A. N. Meckler[1]

[1]Bjerknes Centre for Climate Research and Department of Earth Science, University of Bergen, Norway, [2]Ocean Sciences Department, University of California, Santa Cruz, CA, USA

Abstract The Indo-Pacific Warm Pool (IPWP) plays a crucial role in influencing climate dynamics both in the tropics and globally. Yet, there is an ongoing controversy concerning the evolution of surface temperatures in the IPWP since the Pliocene, which is fueled by contradictory proxy evidence. Temperature reconstructions using TEX_{86} indicate a gradual cooling by ~2°C from the Pliocene to today while Mg/Ca-based studies using planktonic foraminifera do not report any long-term trends. A bias in Mg/Ca records due to seawater chemistry changes has been suggested as an explanation for this proxy mismatch. Here, we present data from two independent foraminifera-based temperature proxies, Mg/Ca and clumped isotopes (Δ_{47}), measured on the same samples from IODP Site U1488 in the IPWP. We reconstructed mixed layer and subsurface temperatures and find very good agreement among Mg/Ca and Δ_{47} when applying a minor correction for changing Mg/Ca ratios of seawater. Diagenetic effects could influence Δ_{47} but the evaluation of foraminifera preservation at Site U1488 suggests that this effect is unlikely to have masked a long-term trend in the data. While remaining uncertainties prevent us from fully ruling out particular hypotheses, our study adds evidence that mixed layer temperatures likely did not cool substantially, while subsurface temperatures cooled more strongly since the Pliocene. The substantial Pleistocene cooling previously observed in TEX_{86} data is consistent with this finding when interpreting it as a combined surface and subsurface signal.

Plain Language Summary Although the Indo-Pacific Warm Pool (IPWP) is a major player within the global climate system, our understanding of sea surface temperatures in the Indo-Pacific Warm Pool (IPWP) since the Pliocene (5.3–2.6 Million years ago) is limited. Various methods to reconstruct past ocean temperatures disagree on the long-term temperature evolution in this region. Studies using the TEX_{86} paleothermometer indicate a ~2°C surface ocean cooling while the Mg/Ca-based temperature reconstructions lack a clear long-term trend since the Pliocene. Different sources of uncertainty can potentially explain this mismatch, including ocean chemistry changes influencing Mg/Ca or differences in the water depth represented by the different proxy signals. Here, we present data from two independent geochemical methods (Mg/Ca and clumped isotopes: Δ_{47}), using the shells of two species of marine microplankton called foraminifera, representing two different water depths. Reconstructing surface and subsurface ocean temperatures in the IPWP we find good agreement between both methods when correcting the Mg/Ca data for minor ocean chemistry changes. While uncertainties remain, our data argue against a substantially warmer Pliocene surface ocean but show a marked cooling of subsurface temperatures. The clear difference between surface and subsurface evolution can reconcile previous proxy data if they represent different water depths.

1. Introduction

The Pliocene, with atmospheric CO_2 levels estimated to be between 300 and 450 ppm (Foster et al., 2017), similar to present-day levels, has received considerable attention as an analogue for near future global climate change under moderate greenhouse gas emission scenarios (Burke et al., 2018; Dowsett et al., 2012; Haywood et al., 2011; Tierney, Haywood, et al., 2019). Within the climate system, the Indo-Pacific Warm Pool (IPWP) acts as a major player both regionally and globally through teleconnections. These teleconnections include the transport of warm water across the Indonesian Archipelago and to higher latitudes via the

global overturning circulation and alterations of air temperature and precipitation patterns as part of the large-scale atmospheric Hadley and Walker circulations (e.g., Molnar & Cane, 2002; Neale & Slingo, 2003). Thus, reconstructions of the temperature of this large body of warm water during the Pliocene is of vital importance to our understanding of climate dynamics both during the Pliocene epoch and in the coming decades (McClymont et al., 2020).

The current knowledge about IPWP climate during the Pliocene and the evolution of the warm pool on geological timescales is based on several climate proxies. These include foraminifera-based methods such as stable oxygen isotope ($\delta^{18}O$) and Mg/Ca records (Ford & Ravelo, 2019; Ford et al., 2015; Jansen et al., 1993; Medina-Elizalde & Lea, 2010; Wara et al., 2005) and biomarkers $U^{K'}_{37}$ and $TEX_{86,}$ which are related to marine nannoplankton and archaea, respectively (O'Brien et al., 2014; Tierney, Haywood, et al., 2019; Zhang et al., 2014).

Wara et al. (2005) concluded based on Mg/Ca analysis on the mixed layer-dwelling foraminifera species *Trilobatus trilobus* that surface water temperatures in the central IPWP remained relatively constant across the Plio-Pleistocene. In combination with evidence for substantial cooling in the eastern equatorial Pacific (Wara et al., 2005), this led to the hypothesis of a Pliocene permanent El Niño-like state (weakened Walker circulation), characterized by a depressed zonal sea surface temperature gradient in the equatorial Pacific ocean (Brierley et al., 2009; Chaisson & Ravelo, 2000; Fedorov et al., 2006, 2010; Ravelo et al., 2006; Wara et al., 2005). Recent data compilations show that the exact magnitude of the reconstructed Pliocene temperature gradient depends on the time window within the Pliocene selected for comparison, which proxy data is used and how they are analyzed (McClymont et al., 2020). Nonetheless, there is agreement that the equatorial temperature gradient was reduced during the Pliocene (Tierney, Haywood, et al., 2019; Wycech et al., 2020), mainly because there is unequivocal evidence that the East Pacific cold tongue was considerably warmer than today in the Pliocene. Thus, the debate centers on data from the west, specifically, the Mg/Ca-based evidence that indicates that the IPWP was not warmer than today in the Pliocene (Wara et al., 2005).

In contrast to the studies using Mg/Ca-based temperature estimates, TEX_{86}-based temperature reconstructions found evidence for a long-term cooling trend in the IPWP from the Miocene to present with Pliocene sea surface temperatures (SSTs) about 2°C warmer than the Late Pleistocene (O'Brien et al., 2014; Zhang et al., 2014). Several potential causes of the observed mismatch between Mg/Ca and TEX_{86}-based temperature reconstructions such as past ocean chemistry changes and the origin of the biomarker signal in the water column are a matter of debate. Although magnesium and calcium behave conservatively in the ocean and Mg/Ca ratios of seawater (Mg/Ca_{sw}) are thus homogeneous, they can vary on geological time scales >1 Myrs (Fantle & DePaolo, 2006). Because the Mg/Ca ratio of marine microfossils depends not only on temperature but also the Mg/Ca_{sw}, variations of the ocean Mg/Ca reservoir can bias temperature reconstructions if not accounted for (e.g., Medina-Elizalde et al., 2008). Considerable effort has been made to quantify past Mg/Ca_{sw} changes on various time scales (e.g., Coggon et al., 2010; Evans et al., 2016; Fantle & DePaolo, 2006; Lowenstein et al., 2001; Stanley & Hardie, 1998; Tierney, Malevich, et al., 2019; Wit et al., 2017). Yet, past Mg/Ca_{sw} ratios reconstructed using different methods are plagued by large uncertainties (see O'Brien et al., 2014). Moreover, some Mg/Ca_{sw} reconstructions are back-calculated from biomarker and Mg/Ca records based on the assumption that the both records depict similar ocean temperature changes (Evans et al., 2016; O'Brien et al., 2014). The accuracy of TEX_{86}-based SST reconstructions in the IPWP, however, has been put into question as well (e.g., Ford et al., 2015). Uncertainties regarding the depth of the TEX_{86} signal complicate the interpretation of TEX_{86} records (reviewed in Schouten et al., 2013). Most notably, recent studies indicate that GDGT (Glycerol dialkyl glycerol tetraether) production beneath the surface is reflected in TEX_{86} temperature calibration data and/or reconstructions (Ho & Laepple, 2016; Kim et al., 2012; Richey & Tierney, 2016; Tierney & Tingley, 2015; Zhang & Liu, 2018). Some studies utilize TEX_{86} as indicators of changes in subsurface temperature and/or changes in vertical water column structure (Hertzberg et al., 2016; Liddy et al., 2016; Seki et al., 2012). In addition, there is evidence that the TEX_{86} record can be influenced by changes in the ecology and community structure of the planktonic archaea producing the signal (Kim et al., 2015; Polik et al., 2018).

To date, the described discrepancy among the two proxies has not yet been resolved due to the lack of an independent way to constrain Pliocene ocean temperatures in the warm pool on million-year timescales. The

$U^{K'}_{37}$ alkenone unsaturation index, another common paleo-thermometer, is hindered by the proxy's upper temperature limit of about 29°C (Müller et al., 1998), although the reconstruction of higher temperatures with larger uncertainties is possible using a novel Bayesian calibration model (Tierney & Tingley, 2018). Applying this calibration to $U^{K'}_{37}$ data from the central IPWP Tierney, Haywood, et al. (2019) found relatively constant maximum temperatures since the Pliocene. These results should be interpreted with care, however, as temperatures much warmer than today might be difficult to detect with this proxy. The $\delta^{18}O$ signal in planktonic foraminifera cannot be used to resolve the observed disagreement among proxies because of this proxy's dependence on the $\delta^{18}O$ of the sea water and hence additional influencing factors such as salinity, precipitation patterns and global ice volume (reviewed in Pearson, 2012; Raymo et al., 2018). In contrast, the clumped isotope (Δ_{47}) proxy provides a unique opportunity to shed new light on this persistent proxy disagreement and help to disentangle the numerous influencing factors on the various temperature records.

The Δ_{47} paleothermometer is based on the fact that the occurrence of doubly substituted (clumped) carbonate ions which contain the two rare isotopes ^{18}O and ^{13}C increases with decreasing formation temperature compared to a purely stochastic distribution (e.g., Schauble et al., 2006). This excess of doubly substituted carbonate ions can therefore be used to calculate the formation temperature of the carbonate (e.g., Eiler, 2007; Eiler & Schauble, 2004; Ghosh et al., 2006; Schauble et al., 2006). While being analytically challenging the major advantage of this temperature proxy is its independence from the isotopic reservoir the carbonate is precipitated from (Eiler, 2007; Ghosh et al., 2006). This means that past changes in the isotopic composition of the ocean do not have to be known in order to apply the Δ_{47} paleothermometer. Furthermore, it has been shown that foraminifera follow the same Δ_{47}-temperature relationship as inorganically precipitated carbonates and no species effects have been observed (Grauel et al., 2013; Meinicke et al., 2020; Peral et al., 2018; Piasecki et al., 2019; Tripati et al., 2010).

Here, we present a long-term (5.6 Ma to present) record of paired Mg/Ca and clumped isotope measurements on the same samples from IODP Site U1488 in the central warm pool. We use our paired measurements on two species of planktonic foraminifera, a mixed layer-dwelling and a deeper-dwelling species, to test various Mg/Ca-temperature calibrations and find the most suitable approach for the site and species investigated here. Furthermore, our independent Δ_{47} record allows us to evaluate the influence of published Mg/Ca_{sw} reconstructions on Mg/Ca records from the IPWP and to address the mismatch between Mg/Ca and TEX_{86}-based temperature reconstructions.

2. Materials and Methods

2.1. Site and Strategy

Site U1488 is located in the southern part of the Eauripik Rise (02°02.59′N, 141°45.29′E, Figure 1) at a water depth of 2,604 m (Rosenthal et al., 2018). The sediment recovered at this site was classified as foraminifera-nannofossil ooze characterized by little variation over time. Bioturbation was described as slight to minor throughout the site. Shipboard preservation analysis using SEM (scanning electron microscope) images revealed excellent to very good preservation in the younger (Pleistocene/Pliocene) part of the sediment with only minor signs of dissolution, very minor textural alteration indicative of early stages of recrystallization, minor secondary calcite overgrowth, and no infillings or cementation. In the youngest part of the Miocene (~7.42–7.49 Ma) good to very good preservation was reported. These samples were characterized by the presence of some dissolution, minor signs of early recrystallization, minor secondary calcite overgrowth and minor infillings of unconsolidated sediment. Preservation was described as getting progressively worse throughout the Miocene. Based on this analysis, we consider sediments younger than 7.42 Ma suitable for foraminifera-based paleotemperature reconstructions.

Our age model rests preferentially on shipboard paleomagnetic data. For the older sections we used selected nannofossil biostratigraphic events as tie points (Supplement Table S1, Drury et al., 2021). Based on this age model we chose nine time intervals over the last 5.6 Myrs in order to reconstruct the long term evolution of central IPWP temperatures. These time intervals are centered around 0.1, 1.0, 1.8, 2.6, 3.2, 3.3, 4.1, 5.1, and 5.6 Ma. Samples for each time interval were selected to roughly cover 100 kyrs or 40 kyrs (0–1 Ma and 1–6 Ma, respectively), to avoid aliasing effects on glacial-interglacial time scales as a result of the relatively large uncertainty of our age model. We note, however, that the uncertainty of our age model does in most

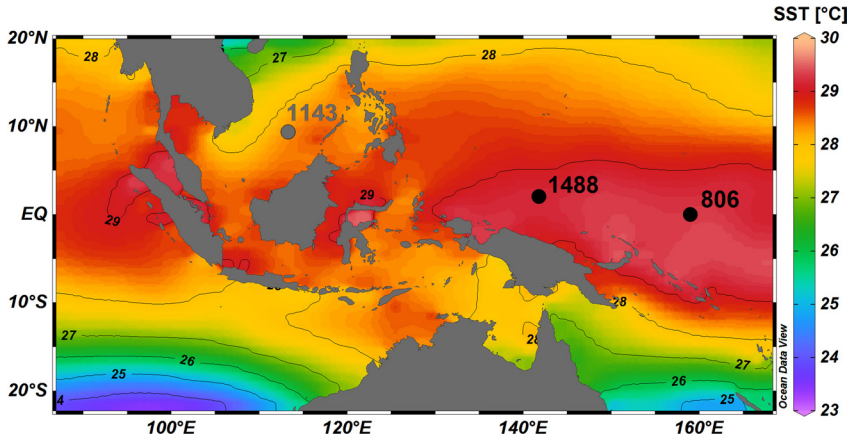

Figure 1. Present-day annual mean sea surface temperature map across the Indo-Pacific Warm Pool displaying the location of Sites 806 and U1488 discussed in this study (black filled circles) and Site 1143 located on the edge of the warm pool (gray filled circle). The temperature information from the World Ocean Atlas (Locarnini et al., 2010) represents a five decade average (1955–2006). Map generated using Ocean Data View (ODV, Schlitzer, 2018).

cases not allow determining the age of any sample on an orbital time scale. Younger (100 kyr) intervals contain ~25 individual samples, 40 kyr intervals ~20. We measured clumped isotopes on every other sample for most time intervals except for the youngest time interval, which we analyzed in full resolution. Mg/Ca was measured on every sample.

We compared our results from Site U1488 to the available Mg/Ca (Wara et al., 2005), TEX_{86} (Zhang et al., 2014) and $U^{K'}_{37}$ data (Etourneau et al., 2010; Pagani et al., 2010; Zhang et al., 2014; recalculated by Tierney, Haywood, et al., 2019) from Site 806 which is also located in the central IPWP (Figure 1) and was likely subject to similar environmental conditions during the last 5.6 Myrs. We refrain from including data from Site 1143 in this direct comparison as this site today is located on the edge of the warm pool but might have been influenced by a laterally expanded Pliocene IPWP (Brierley et al., 2009).

2.2. Species of Planktonic Foraminifera

The two species of planktonic foraminifera analyzed for both Mg/Ca and Δ_{47} in this study were selected to meet two main criteria: Both species should be abundant throughout all time intervals from 5.6 Myrs to present and the two species should represent mixed layer and thermocline temperatures, respectively.

The species *Trilobatus trilobus* formerly known as *Globigerinoides trilobus* or *G. sacculifer* without sac-like final chamber (Spezzaferri et al., 2015) is a mixed layer-dwelling species commonly used for paleoceanographic studies (e.g. Wara et al., 2005). *T. trilobus* are widespread close to the sea surface in tropical and subtropical oceans (Bé & Tolderlund, 1971; Schmuker & Schiebel, 2002). They are frequently the dominant species of the faunal assemblage, especially in oligotrophic waters (Bijma & Hemleben, 1994). The depth habitat of this species is restricted to the mixed layer (reviewed in Schmidt et al., 2016) with larger specimens (>300 μm) occupying a depth habitat of roughly 50–75 m (e.g., Bijma & Hemleben, 1994). However, for the Manihiki Plateau in the equatorial Pacific Ocean unusually deep calcification depths (~120 m) were described (Rippert et al., 2016). If this was the case at Site U1488 as well, we would expect to reconstruct lower mixed layer temperatures rather than SSTs.

The second species we used, *Globorotalia tumida,* is found in tropical to subtropical oceans in relatively low abundance. It is associated with the seasonal thermocline at low latitudes (Ravelo et al., 1990; Ravelo & Fairbanks, 1992). Interpreting the oxygen isotope signal measured in *G. tumida* from the Atlantic Ocean, Cléroux et al. (2013) estimated an apparent calcification depth of 145 or 160 m (depending on the calibration). Farmer et al. (2007) calculated even deeper calcification depths (176–273 m), below the thermocline for *G. tumida* from several sites in the same ocean basin. This species may form a thick calcite crust deeper in the water column (reviewed in Schiebel & Hemleben, 2017).

2.3. Sample Treatment

Sample pretreatment for both Mg/Ca and Δ_{47} was done at the University of Bergen. All samples were wet-sieved over a 63 μm sieve and dried at ≤50°C. Further separation of individual size fractions within the coarse fraction was done by dry-sieving. We picked the mixed layer-dwelling planktonic foraminifera species *T. trilobus* and thermocline-dwelling *G. tumida* from the 355–425 μm fraction. For each sample and species, approximately 30 and 60 specimens were selected under the microscope for Mg/Ca and clumped isotope analyses, respectively. The preservation of all individual specimens was assessed under the microscope and only fully intact pristine-looking tests without substantial infillings or oxide coatings were selected for analysis. For *T. trilobus* translucent specimens were preferred for analysis where available.

Deeper-dwelling globorotalid species such as *G. tumida* commonly feature secondary calcite crusts and encrusted specimens are known to reveal different isotopic and trace element compositions (Hemleben et al., 1985; Lohmann, 1995). Specimens of *G. tumida* without secondary calcite crusts were not available in sufficient amounts throughout all time intervals. In order to avoid any biases in the reconstructed temperatures between samples with and without encrustation we decided to use generally well preserved but moderately encrusted specimens of *G. tumida* throughout the site. We expect encrusted specimens to exhibit somewhat deeper apparent calcification depth than pristine-looking specimens without any encrustation. SEM images were used for each time interval to further assess the preservation state of individual samples including signs of diagenetic overprinting such as dissolution, secondary calcite precipitation and recrystallization.

Mg/Ca measurements were performed at the *University of California, Santa Cruz (UCSC)*, Δ_{47} and stable oxygen isotopes ($\delta^{18}O$) were measured at the University of Bergen.

2.4. Clumped Isotope Analysis

On average, 36 specimens of *T. trilobus* (1.2 mg) or 19 specimens of *G. tumida* (1.2 mg) were measured per sample for Δ_{47} analysis. We cleaned batches of around 30–35 and 15–20 specimens of *T. trilobus* and *G. tumida*, respectively. To crack open all individual chambers and allow for subsequent cleaning we carefully crushed the foraminifera between two glass plates. The crushed tests were sonicated several times for 5 s each, first with DI water, then with methanol followed by two more sonication steps with DI water. After each sonication step the samples were rinsed with DI water. The cleaned samples were then dried in an oven at ≤50°C. SEM images taken on some of the samples before and after cleaning were used to verify that the cleaning removed any contaminants on the outside of the tests while preserving the structure of the foraminifera tests.

Oxygen and clumped isotope measurements were carried out using one of two Thermo Scientific MAT 253Plus mass spectrometers coupled to KIEL IV carbonate devices (Thermo Fisher Scientific, Bremen, Germany). The Kiel device was operated with a Porapak trap used to remove organic contaminants (Schmid & Bernasconi, 2010). Depending on the mass spectrometer used for each replicate the Porapak trap was operated either at −20°C or −40°C. The trap was heated to 150°C for at least one hour each day for cleaning. All replicates were reacted individually in the Kiel device with phosphoric acid (reaction temperature: 70°C).

To address the large analytical uncertainty associated with individual Δ_{47} measurements, >20 replicate measurements are needed for a temperature reconstruction with an uncertainty of 1.5°C (68% confidence interval) or less (Meinicke et al., 2020). We measured 6 to 16 (average $n = 8$) replicates (85–135 μg each) for every sample. Mean values for $\delta^{18}O$ and Δ_{47} were then calculated from the individual replicate measurements per sample. Additionally, average Δ_{47} values for each time interval were determined from all aliquot measurements within that interval. Temperature uncertainties were calculated as 68% and 95% confidence intervals based on a Monte Carlo approach including the analytical and the calibration uncertainty.

The long-integration dual-inlet (LIDI) method described by Hu et al. (2014) was used for the measurement with 400 s integration time per analysis. Various corrections including a pressure baseline correction (Bernasconi et al., 2013; Meckler et al., 2014), a ^{17}O correction (described in Daëron et al., 2016; Schauer et al., 2016) and the transfer into the absolute reference frame (Dennis et al., 2011) were applied to the data

using the Easotope software package (John & Bowen, 2016). The process is described in greater detail in Piasecki et al. (2019); Meinicke et al. (2020).

All sample measurements were accompanied by roughly equal numbers of carbonate standard measurements (values reported in Bernasconi et al., 2018). To account for potential future methodological improvements making it necessary to recalculate the values from this study, we will provide replicate-level raw data in the EarthChem database (https://www.earthchem.org/). The carbonate standards ETH1 to ETH3 were used to transfer the results into the absolute reference frame (Dennis et al., 2011). ETH 4 was used to monitor the corrections. The quality of the pressure baseline correction was monitored using long-term averages of ETH 1 and 2 (see Bernasconi et al., 2018) and baseline-corrected Δ_{48} values served as a contamination monitor (none of the samples showed signs of contamination). The average standard deviation (1SD) of the Δ_{47} values determined for the final carbonate standard results was used to monitor the long-term reproducibility. Across the whole measuring interval standard deviations of the four different carbonate standards were between 0.036‰ and 0.039‰ (Supplement Table S2). A total number of 60 standard measurements from the same and adjacent days was used for the corrections applied to each replicate measurement. The exact number of standards for the corrections was chosen based on the instrument stability during the respective time interval (see Piasecki et al., 2019 for more information). In addition to the drift correction using the ETH carbonate standards we also aimed to distribute the individual replicate measurements for our samples over long time intervals. The $\delta^{18}O$ values measured along with Δ_{47} were corrected for drift and scale compression using the same ETH carbonate standards. These have been referenced to NBS18, NBS19 and LSVEC (see Bernasconi et al., 2018).

We used the Δ_{47}-temperature calibration published by Meinicke et al. (2020) to calculate formation temperatures of the two species of planktonic foraminifera. The global multi-species calibration is based on data from 14 species of foraminifera, including the two species analyzed in this study. The chosen calibration includes data from two additional recent calibration studies using foraminifera (Peral et al., 2018; Piasecki et al., 2019) and therefore represents the most extensive clumped isotope data set using foraminifera to date. Moreover, this calibration agrees well with recent inorganic Δ_{47}-temperature calibrations. Temperatures were calculated using the combined calibration (Meinicke et al., 2020, Equation 2) which is also based on the same carbonate standards that were used for standardization in this study. Δ_{47} values for both the calibration and our samples were originally derived using values for ETH1-3 as published by Bernasconi et al. (2018). However, thanks to a community-wide effort to improve inter-laboratory comparison, the accepted values for these standards have recently been updated (I-CDES scale; Bernasconi et al., 2021). Although measured prior to this recent advance, our Δ_{47} data were fully recalculated using the updated standard values and reported on the I-CDES scale. The final Δ_{47} values were transferred to calcification temperatures by means of the following, recalculated version of the foraminifera-based calibration by Meinicke et al. (2020):

$$\Delta_{47} = \left(0.0397 \pm 0.0011\right) * \frac{10^6}{T^2} + \left(0.1518 \pm 0.0128\right) \quad (1)$$

This recalculated version of the calibration by Meinicke et al. (2020) should be used instead of the original version (Meinicke et al., 2020, Equation 2) for future studies that are based on the I-CDES scale proposed by Bernasconi et al. (2021).

For maximum compatibility, we included both the original and the recalculated final Δ_{47} values for Site U1488 in the EarthChem database (https://doi.org/10.26022/IEDA/111920). Note that temperature estimates generated from fully recalculated data using Equation 1 are warmer by 0.7°C –0.9°C than temperatures calculated from the original data.

2.5. Mg/Ca Analysis

Planktonic foraminifera of the mixed layer-dwelling species *T. trilobus* (all nine time intervals) and the thermocline-dwelling species *G. tumida* (four time intervals) were analyzed for minor element ratios (Mg/Ca, Sr/Ca, Mn/Ca) at UCSC. Within each time interval, 20–25 samples (depending on the length of the glacial-interglacial cycle, see Section 2.1) were analyzed. Per sample, approximately 20-30 specimens of

T. trilobus and ~20 specimens of *G. tumida* were crushed and cleaned for analysis. The cleaning protocol included sonication in Milli-Q and methanol, and a trace-metal cleaning with reductive and oxidative reagents (Martin & Lea, 2002). Cleaned samples were transferred to acid-cleaned vials and analyzed for minor element ratios using a ThermoFisher iCAP 7400 ICP-OES. A liquid consistency standard which was used to monitor the long-term reproducibility of the instrument yielded 3.28 ± 0.08 mmol/mol (1σ, n = 167). Additionally, two internal standards revealed a reproducibility of 3.75 ± 0.18 mmol/mol (*T. trilobus*, 1σ, n = 33) and 2.28 ± 0.23 mmol/mol (*Pulleniatina obliquiloculata*, 1σ, n = 26). The choice of Mg/Ca-temperature calibration is discussed in Section 4.1.

2.6. Diagenesis Model

In order to appraise the effect of potential diagenetic overprinting, we use a linear mixing model with two endmembers. Our model assumes that the Δ_{47} signal records the temperature signal during foraminifera test formation and may get overprinted by secondary calcite formed under bottom water or pore water temperature (depending on the depth in the sediment that this secondary calcite is formed).

Although Δ_{47} mixing is a non-linear process when the $\delta^{18}O$ and $\delta^{13}C$ composition of the end members differ substantially (e.g., Defliese & Lohmann, 2015; Eiler & Schauble, 2004), non-linear mixing effects can be neglected for sediments where $\delta^{13}C$ values of the original calcite and diagenetic carbonate are comparable (Leutert et al., 2019; Stolper et al., 2018). Stolper et al. (2018) discussed potential non-linearity effects for Site 807 from the Western Pacific Warm Pool and decided that a linear mixing model is sufficient to approximate diagenetic processes in this setting. Following this interpretation, we also decided to neglect non-linearity effects.

Equation 2 was used to describe mixing between the Δ_{47} signature of pristine surface water calcite ($\Delta_{47\,\text{pristine}}$) and Δ_{47} of diagenetic calcite ($\Delta_{47\,\text{diag}}$) formed either at the bottom water-sediment interface or deeper in the sediment. The mixed signal ($\Delta_{47\,\text{foram}}$) in this model only depends on the temperature of the two endmembers and the fraction of diagenetic calcite (F_{diag}):

$$\Delta_{47\,\text{foram}} = F_{\text{diag}} * \Delta_{47\,\text{diag}} + \left(1 - F_{\text{diag}}\right) * \Delta_{47\,\text{pristine}} \quad (2)$$

The Mg/Ca-based mixed layer temperature (without and with different Mg/Ca_{sw} corrections) was used as pristine surface temperature while the Mg/Ca temperature from benthic foraminifera at Site 806 (Lear et al., 2015) was taken as the temperature at the bottom water-sediment interface. We acknowledge a significant uncertainty associated with the timing of diagenetic processes. The majority of diagenetic calcite could be formed very early after deposition at bottom water temperatures, or much later at the final burial depth, or gradually during deposition and burial. Therefore, we calculated the diagenetic fractions for two extreme scenarios: (a) instantaneous diagenesis at bottom water temperatures (smallest fraction of diagenetic calcite) and (b) 100% of diagenesis occurring at the final burial depth (largest fraction). Because the geothermal gradient in this region is estimated to be 25–35 K/km (Schrag et al., 1995), we used a conservative estimate of 25 K/km for our calculations.

3. Results

The Δ_{47} and $\delta^{18}O$ values were determined for eight (*T. trilobus*) and four (*G. tumida*) time intervals across the last 5.6 Myrs. Except for the *T. trilobus* samples in the youngest time interval, where we measured 24 samples across ~100 kyrs, we analyzed between 9 and 13 samples per time interval (Supplement, Table S3).

The $\delta^{18}O$ signal of *T. trilobus* ranges between −2.23 and −0.68‰ (Figure 2a) lacking a discernible long-term trend. The youngest time interval is characterized by the largest $\delta^{18}O$ range among the individual samples, with most negative $\delta^{18}O$ (−2.23‰) in the youngest samples and highest values (−0.68‰) during the Last Glacial Maximum (LGM). The individual samples of the thermocline-dwelling *G. tumida* are characterized by an increasing trend in $\delta^{18}O$ values from −1.42 to −1.00 at 4.1 Ma to values between −0.74 and +0.74‰ within the youngest time interval.

We calculated mean Δ_{47} values for each time interval to average over full orbital cycles and achieve robust average temperature estimates from ≥70 individual measurements (Figure 2b, Supplement Table S3). The

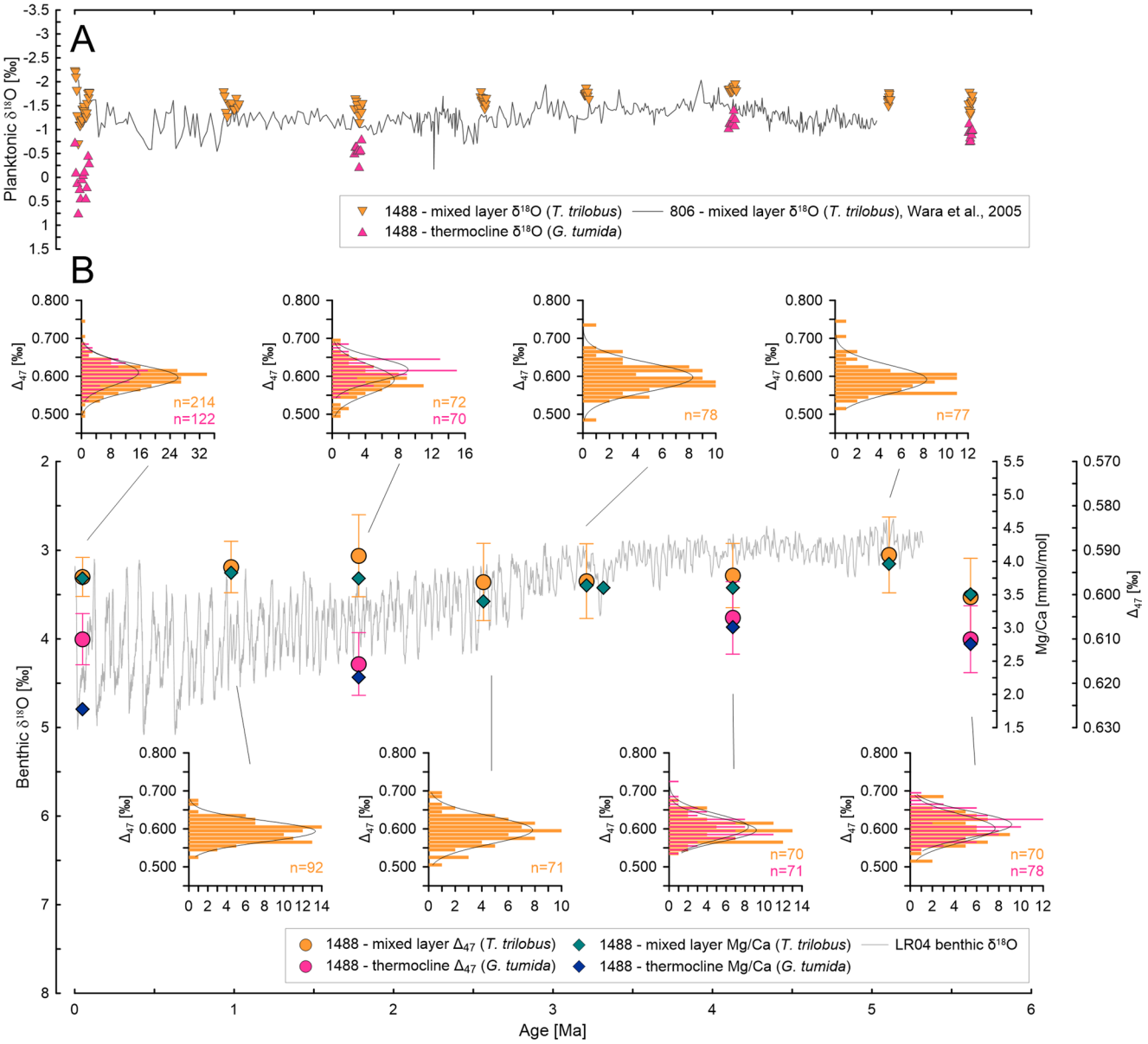

Figure 2. Average mixed layer (*T. trilobus*) and thermocline (*G. tumida*) $\delta^{18}O$ and Mg/Ca ratios and Δ_{47} values for the time intervals distributed across the last 5.6 Myrs. (a) Mixed layer *T. trilobus* (orange filled triangles) and thermocline *G. tumida* (magenta filled triangles) $\delta^{18}O$ displayed against the Site 806 mixed layer $\delta^{18}O$ record (black line, Wara et al., 2005) using the updated age model presented in Ford et al. (2015). (b) Mg/Ca ratios are shown as green (*T. trilobus*) and dark blue (*G. tumida*) filled diamonds. Clumped isotope measurements are presented as average Δ_{47} values of *T. trilobus* (orange filled circles) and *G. tumida* (magenta filled circles) and as histograms illustrating the distribution of all individual replicate measurements for the selected time intervals. The number of individual Δ_{47} measurements (n) is shown for each time interval and species, and normal distribution fits are plotted for each histogram. Error bars represent two standard errors of the average Δ_{47} values for each interval. The LR04 benthic $\delta^{18}O$ stack (Lisiecki & Raymo, 2005) is shown for reference (gray line).

results of the individual aliquots and the number of aliquots measured per time interval are displayed for both species as histograms (Figure 2). The distribution of individual measurement results within each time interval roughly follows a normal distribution highlighting the random nature of the analytical uncertainty on the Δ_{47} measurement. The average Δ_{47} ratios for *T. trilobus* range between 0.666 and 0.677‰ (standard error of the mean ≤0.005‰) and do not reveal any long-term trends. *G. tumida* reveals generally higher Δ_{47} (0.683–0.693‰, standard error ≤ 0.004‰) across the four intervals analyzed compared to *T. trilobus*, corresponding to lower temperatures. The average Δ_{47} values and standard errors calculated for the time intervals correspond to analytical uncertainties ≤1.5°C.

The patterns found in the $\delta^{18}O$ signal are also reflected in the Mg/Ca values for both species: We measured Mg/Ca ratios across nine time intervals for surface-dwelling *T. trilobus* and four intervals for the thermocline species *G. tumida*. For comparison with the Δ_{47} values, we also calculated mean interval Mg/Ca temperatures (Supplement Table S3). Mean Mg/Ca ratios for *T. trilobus* (Figure 2b) range between 3.4 and 4.0 mmol/mol (SD across individual time intervals ≤0.4 mmol/mol) and show no long-term trend during the last 5.6 Myrs. The ratios determined for *G. tumida* on the other hand range between 1.8 and 3.0 mmol/mol (SD across individual time intervals ≤0.2 mmol/mol) and suggest lower values for the younger time intervals compared to the older ones. Mn/Ca ratios for both species range between 0 and 0.6 and 0 and 0.3 mmol/mol for *T. trilobus* and *G. tumida*, respectively. Sr/Ca ratios vary between 1.1 mmol/mol and 1.4 mmol/mol for both species. Along with the Mg/Ca ratios and isotope data of each individual sample Mn/Ca and Sr/Ca data can be found on Pangaea (https://doi.org/10.1594/PANGAEA.933340).

4. Discussion

4.1. Assessment of Mg/Ca Calibrations

There are different approaches to generate marine paleotemperature calibrations. One group of calibration studies relates the proxy signal to SST (e.g., Tierney, Malevich, et al., 2019), even though the temperature signal might be produced deeper in the water column. The advantage of this approach is that the result is directly comparable to estimates derived from other proxies. However, the implicit assumption has to be made that the depth of signal production at the sites used for calibration is representative of the sites where the proxy is applied, that the relationship between that temperature and SST is similar, and that both relationships are stable over time. Foraminifera, for example, are known not only to occupy species-specific depth habitats but may also move laterally in the water column throughout their life cycle (e.g., Emiliani, 1954). This ecological behavior may also vary regionally (e.g., Pujol & Grazzini, 1995). As a result the temperature-related geochemical information recorded in foraminifera tests represents a mixed signal across the range of water depths occupied by the analyzed specimens (reviewed in Pearson, 2012; see also Ford & Ravelo, 2019). Therefore, a second approach for temperature calibrations relates the proxy signal to the temperature at the assumed production depth rather than SST (e.g., Anand et al., 2003; Dekens et al., 2002).

With respect to identifying a suitable Mg/Ca-temperature calibration for *T. trilobus*, we decided to focus on calibrations relating Mg/Ca to calcification temperatures within the mixed layer rather than SST. This approach has several advantages for our purpose: First, the Δ_{47} data that the Mg/Ca record is compared to also reflect calcification temperatures. Calculating mixed layer temperatures from the *T. trilobus* Mg/Ca record thus allows for a direct comparison between these two foraminifera-based methods, independent of potential biological effects. With Δ_{47}, we add another source of temperature information to the foraminifera data which is independent of seawater chemistry and can therefore be used to test our Mg/Ca data treatment. Second, the species analyzed here appears to calcify relatively deep in the water column in the warm pool, possibly deeper than at other sites (e.g., Rippert et al., 2016), potentially violating the equivalency to the signal production depth at calibration sites. Third, although the calibration of *T. trilobus* to mixed layer temperatures impedes a comparison to SST records from other proxies and model-derived SST, we see significant value in being able to reconstruct the thermal structure in the water column with a combination of proxies.

We use the results from the youngest interval to assess a range of calibrations for $\delta^{18}O$ and Mg/Ca for *T. trilobus*, in comparison to Δ_{47} and present-day temperatures (Figure 3). For estimating Holocene temperatures from $\delta^{18}O$, an average $\delta^{18}O_{sw}$ value (of 0.31‰) for the upper 100 m of the water column at Site U1488 (LeGrande & Schmidt, 2006) was used for the temperature calculation. The $\delta^{18}O$-T calibrations of Erez and Luz (1983), Kim and O'Neil (1997) and the calibration published by Bemis et al. (1998) for high light conditions were selected for this comparison; these are all multi-species calibrations commonly applied in paleoceanographic studies.

For mixed layer temperatures based on Mg/Ca we tested two widely used calibrations from Anand et al. (2003) and Dekens et al. (2002) and a recent calibration by Gray and Evans (2019). The Anand et al. (2003) calibration can be used for multiple species whereas the other two calibrations used here provide species-specific equations for *T. trilobus* (Dekens et al., 2002) and *T. sacculifer* (Gray & Evans, 2019) which belongs to the same biologic species as *T. trilobus* (André et al., 2013; Bijma & Hemleben, 1994; Spezzaferri et al., 2015).

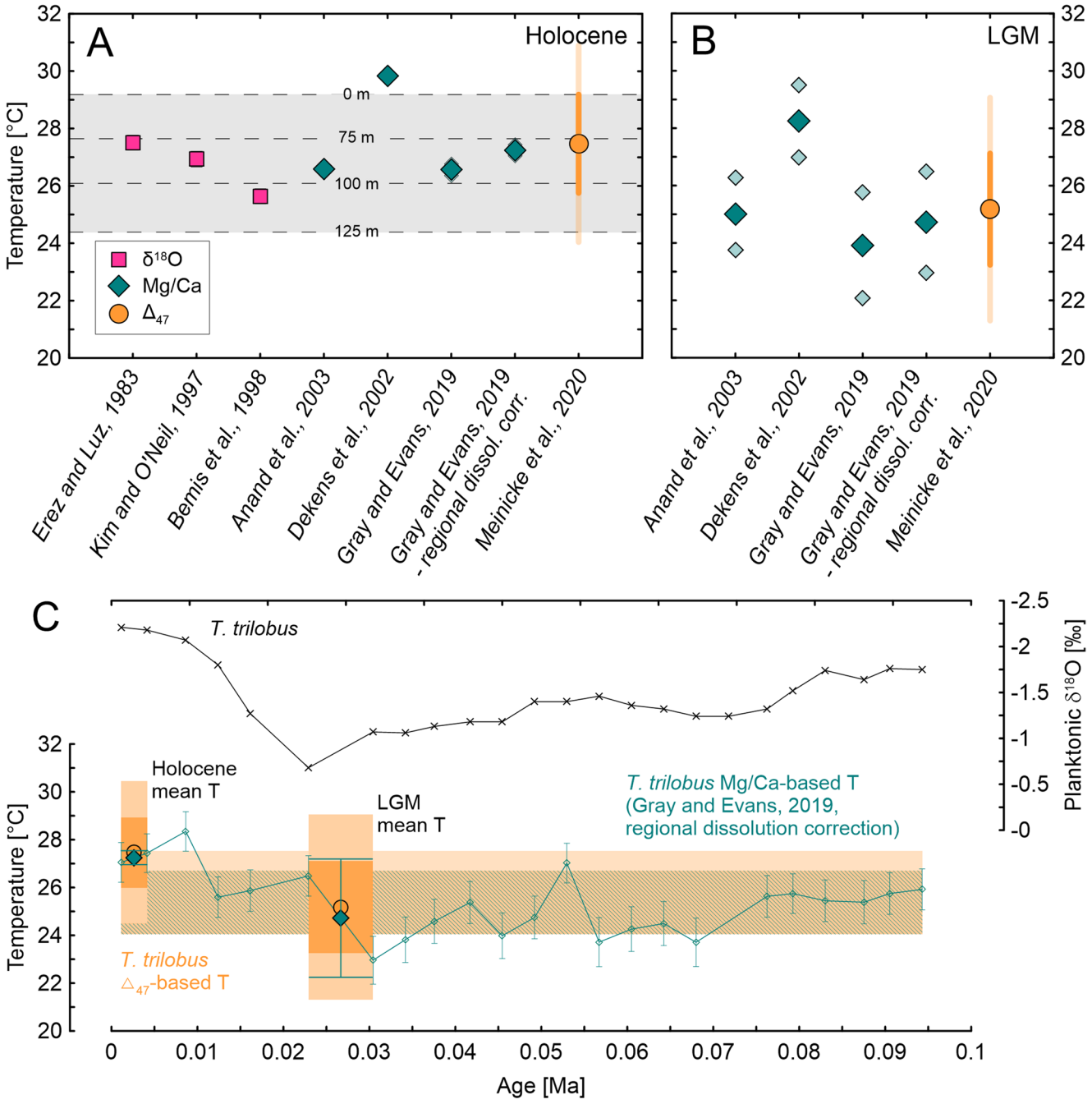

Figure 3. Proxy information for the youngest time interval based on the mixed layer-dwelling foraminifera species *T. trilobus*: (a) Holocene comparison of different calibrations for $\delta^{18}O$ (Erez & Luz, 1983; Kim & O'Neil, 1997; Bemis et al., 1998, magenta squares), Mg/Ca (Anand et al., 2003; Dekens et al., 2002; Gray & Evans, 2019, individual samples and mean Holocene values shown as light and dark green diamonds, respectively) and Δ_{47} (Meinicke et al., 2020, orange filled circles). The gray shaded area represents the annual mean water temperature between 0 and 125 m at this site (Locarnini et al., 2010). (b) LGM comparison of Mg/Ca (Anand et al., 2003; Dekens et al., 2002; Gray & Evans, 2019, individual samples and mean LGM values shown as light and dark green diamonds, respectively) and Δ_{47} (Meinicke et al., 2020, orange filled circles) temperatures. (c) Planktonic $\delta^{18}O$ (black line) and Mg/Ca-based temperatures (green line) for all samples in the youngest time interval. Mg/Ca temperatures were calculated using the calibration published by Gray & Evans, 2019 (combined with a regional dissolution correction). Mean temperatures for the whole interval are represented by shaded areas. Orange area: Mean Δ_{47} temperature ±95% confidence intervals. Green area: Mean Mg/Ca temperature ±1SD of the individual samples. Mean Holocene and LGM temperatures (same as in A and B) are displayed by green (Mg/Ca) and orange (Δ_{47}) symbols. Uncertainties are displayed as 68 and 95% confidence intervals (Δ_{47}) and one standard deviation of the individual samples (Mg/Ca).

The advantage of the calibration by Gray and Evans (2019) compared to older studies is that this study accounts for the effects of salinity and pH on the Mg/Ca ratio of foraminifera. Because of its relatively shallow depth of ~2.6 km, above the lysocline (Berger et al., 1982; McCorkle et al., 1995), we assume that Site U1488 is only affected by minor dissolution (see Dekens et al., 2002; Sadekov et al., 2010). Sadekov et al. (2010) presented evidence that *T. trilobus* is not susceptible to large-scale dissolution above the lysocline and suggested that preferential dissolution of high-Mg calcite does not strongly affect this species.

Nonetheless, based on the evidence for a small dissolution effect on *T. trilobus* at the nearby Ontong Java Plateau (Dekens et al., 2002), we decided to follow the approach by Dyez and Ravelo (2013) and apply small dissolution correction to Site U1488. This correction uses the regional depth-dissolution relationship determined from core-tops from the Ontong Java Plateau (Dekens et al., 2002) to correct for relatively minor effects of dissolution. The correction translates to a 4.2% increase in all measured Mg/Ca ratios which were then converted to temperature using the calibration published by Gray and Evans (2019).

For the Holocene, we find good agreement between Δ_{47} temperatures, $\delta^{18}O$-based temperatures calculated using Erez and Luz (1983), Kim and O'Neil (1997) and Bemis et al. (1998), and Mg/Ca-based temperatures using Anand et al. (2003) and Gray and Evans (2019), either with or without a dissolution correction (Figure 3a). All temperatures except for Mg/Ca-based temperatures calculated using the calibration of Dekens et al. (2002) fall within the range of modern-day annual mean water temperatures between 0 and 125 m (Locarnini et al., 2010). Our data thus indicates an apparent calcification depth of *T. trilobus* at this site within the lower mixed layer. Temperatures calculated with the calibration of Dekens et al. (2002) on the other hand appear too warm for *T. trilobus* at Site U1488, due to over-correcting for dissolution and assuming a calcification depth of 20 m for *T. sacculifer*. A more recent study investigating calcification depths of several species in the Western Pacific Warm Pool (Rippert et al., 2016) showed that even shallow-dwelling species such as *T. trilobus* in this region reflect average mixed layer temperatures rather than the warmest temperatures directly at the surface. Hence, calcification temperatures around 30°C, above the annual mean SST (29.2°C, Locarnini et al., 2010), are probably an overestimation.

The LGM was identified based on the age model and confirmed using the planktonic $\delta^{18}O$ values (Figure 3c). As with the Holocene, the LGM data indicate good agreement between temperatures derived from Mg/Ca and Δ_{47}, except for the temperature estimates with the Dekens et al. (2002) calibration. Compared to the other calibrations, those estimates are 3°C–4°C warmer, similar to modern SSTs, which is again unrealistically warm (Figure 3b). We do not calculate $\delta^{18}O$-based temperature estimates due to the unconstrained $\delta^{18}O_{sw}$ for the glacial warm pool mixed layer.

Both the calibrations by Anand et al. (2003) and by Gray and Evans (2019) reproduce modern mixed layer ocean temperatures at the site well and show good agreement with $\delta^{18}O$ and Δ_{47}, and can thus be applied downhole. The recent calibration of Gray and Evans (2019), however, has several advantages for our purpose: This study includes a species-specific calibration for the morphospecies *T. sacculifer* which is assumed to behave very similar to *T. trilobus*. As described by Gray and Evans (2019), their species-specific equations account for different sensitivities among various species to changes in the carbonate chemistry; their study suggests that *T. sacculifer* (and thus also *T. trilobus*) is largely insensitive to carbonate chemistry rendering the reconstruction of pH for our temperature reconstruction unnecessary. The Gray and Evans (2019) calibration also accounts for the variability of salinity over time based on relative sea level changes. We used published Plio-Pleistocene relative sea level changes covering 0–5.3 Ma (Rohling et al., 2014), and changes between 5.3 Ma and 6.0 Ma (Miller et al., 2011) for this purpose. In combination with a dissolution correction, the Gray and Evans (2019) calibration not only leads to an excellent agreement with Δ_{47} temperatures for the Holocene (Figure 3a), the LGM (Figure 3b), and the whole first time interval (Figure 3c), but also accounts for various influences on the Mg/Ca data such as local salinity and pH. We therefore apply the calibration of Gray and Evans (2019) to the *T. trilobus* data from the last 5.6 Myrs to reconstruct the evolution of the IPWP and assess if and how strongly the Mg/Ca data needs to be corrected for long-term Mg/Ca_{sw} variability through comparison with Δ_{47} temperatures. The sensitivity of *T. trilobus* to Mg/Ca_{sw} changes is reasonably well constrained (Evans et al., 2016) allowing to test the influence of different Mg/Ca_{sw} reconstructions on Mg/Ca-based temperature reconstuctions in this species without the need for additional assumptions. We decided to keep the dissolution correction applied to *T. trilobus* Mg/Ca data

constant throughout the record as there is no evidence for a change in dissolution in this region across the Plio-Pleistocene (White & Ravelo, 2020).

In terms of the thermocline species *G. tumida*, there are less options for Mg/Ca temperature calibrations. We decided to use the multi-species calibration published by Anand et al. (2003) without any correction for effects of dissolution since *G. tumida* is described as even more dissolution resistant than *T. trilobus* (Rosenthal & Lohmann, 2002; Schiebel & Hemleben, 2017 and references therein). Using the Anand et al. (2003) calibration for *G. tumida* results in a Holocene temperature of 19.4°C (Figure 6) which is in accordance with today's annual mean water temperature between 150 and 200 m (Locarnini et al., 2010) and thus fits the assumed thermocline habitat depth (depth range: 145–273 m, Cléroux et al., 2013; Farmer et al., 2007). We acknowledge that absolute temperatures may be biased to a certain degree due to the lack of species-specific calibrations. We adopted the approach by Medina-Elizalde et al. (2008) to apply a non-linear correction for changes in Mg/Ca_{sw}. Since no culture experiments are available that determine the response of *G. tumida* to Mg/Ca_{sw} changes for a given temperature, we used the inorganic calcite response as a stand-in (following Medina-Elizalde et al., 2008), which predicts an increase in the partition coefficient of Mg into calcite as Mg/Ca_{sw} decreases (Mucci & Morse, 1983). Different planktonic foraminifera species exhibit different sensitivities to changes in Mg/Ca_{sw}, but based on culturing experiments these responses are typically non-linear and the inorganic calcite response chosen here represents a moderate change in sensitivity (Evans & Müller, 2012 and references therein). Making this assumption for *G. tumida* leads to a stronger correction for Mg/Ca_{sw} changes compared to the correction for *T. trilobus*. Since the variable incorporation of Mg into foraminifera shells is explained by a power component ($H = 0.64$ for inorganic calcite), the exact magnitude of the correction has a large influence on the reconstruction temperatures, introducing uncertainty due to potential systematic under- or overcorrection. Here we aim to validate the Mg/Ca-based calcification temperature estimates with the help of the independently determined Δ_{47} temperatures using the multi-species calibration by Meinicke et al. (2020). However, we acknowledge that independent processes such as past Mg/Ca_{sw} changes or diagenetic alteration could potentially bias Mg/Ca and Δ_{47}-based temperatures in the same direction.

4.2. Mixed Layer Temperature Evolution Since 6 Ma

Over the last 5.6 Myrs, mixed layer Mg/Ca temperatures using the Gray and Evans (2019) calibration without any correction for seawater Mg/Ca changes or dissolution are consistently colder than the Δ_{47}-based temperatures, except in the oldest interval (Figure 4). Applying a regional dissolution correction brings Mg/Ca and Δ_{47} temperatures into good agreement across the last 5.6 Myrs, although Δ_{47} temperatures are still slightly warmer in most intervals, possibly indicating that the dissolution correction on Mg/Ca should be slightly larger. However, due to the uncertainties in Δ_{47} temperatures, an adjustment of this magnitude cannot be justified. Both proxies indicate temperatures between 23°C and 27°C and follow a similar pattern characterized by temperature variability on million-year timescales with lowest temperatures at 2.6 and 5.6 Ma.

Both Mg/Ca and Δ_{47}-based temperature estimates indicate some variability over the last 5.6 Myrs, but no discernible long-term trend in mixed layer temperatures.

The magnitude of an assumed change in past Mg/Ca_{sw} and its effect on reconstructed temperatures varies considerably among studies (Evans et al., 2016; Tierney, Malevich, et al., 2019). The seawater correction published by Evans et al. (2016) leads to progressively warmer temperatures back in time (Figure 4) and thus brings Mg/Ca mixed layer temperatures from *T. trilobus* closer to the TEX_{86}-based SST reconstructions from Sites 806 (Zhang et al., 2014) which indicate a long-term cooling of 2°C–3°C from 6 Ma to present. This is not surprising since 806 TEX_{86} temperatures were themselves used to generate this Mg/Ca_{sw} reconstruction so that the TEX_{86} and resulting Mg/Ca-based temperatures would match. However, our new Δ_{47} data do not support this temperature evolution.

Tierney, Malevich, et al. (2019) suggested a different evolution of Mg/Ca_{sw}, based on a compilation of different datasets, including, for the last 6 Myrs, fossil corals (Gothmann et al., 2015) and fluid inclusions in calcite veins (Coggon et al., 2010). Although these compiled data are characterized by substantial scatter, introducing uncertainty in the derived evolution of Mg/Ca_{sw}, they can be used to correct Mg/Ca-based

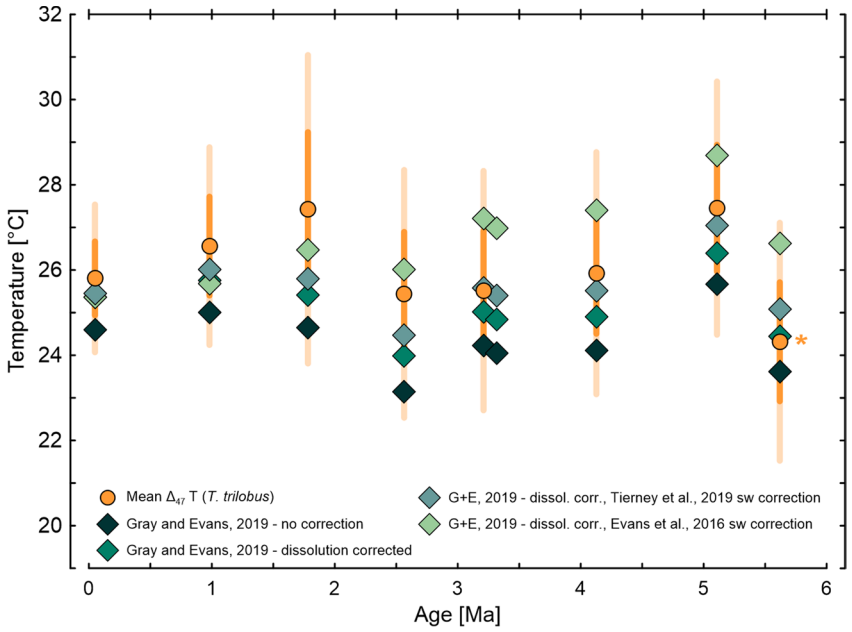

Figure 4. Mixed layer (*T. trilobus*) Δ_{47} temperatures (orange circles) compared to Mg/Ca (green diamonds) corrected in different ways. Different shades of green represent various stages of correcting the Mg/Ca data. Dark green: uncorrected Mg/Ca values, green: Mg/Ca values corrected for dissolution following the approach of Dyez and Ravelo (2013), teal: Mg/Ca values corrected for dissolution and for small Mg/Ca_{sw} changes after Tierney, Malevich, et al., 2019, light green: Mg/Ca values corrected for dissolution and for stronger Mg/Ca_{sw} changes after Evans et al. (2016). Error bars for the Δ_{47} values represent 68% and 95% confidence intervals. The orange asterisk highlights the clumped isotope value potentially affected by a significant amount of diagenetic secondary calcite (see Figure 5).

temperatures without employing circular reasoning. Using this smaller seawater correction proposed by Tierney, Malevich, et al. (2019), which is similar to the Mg/Ca_{sw} estimate based on calcite veins only (Coggon et al., 2010), results in good agreement between Mg/Ca and Δ_{47} temperatures; all mean Mg/Ca-based temperatures fall within the 68% confidence interval of the Δ_{47} temperatures (Figure 4). In order to solve the discrepancy between Mg/Ca, Δ_{47} and TEX_{86}-based temperature estimates, and to assess the magnitude of Mg/Ca_{sw} correction needed across the Plio-Pleistocene, potential additional influences on any of the three proxies (such as depth of GDGT production and calcite diagenesis) need to be considered. Two contrasting hypotheses (Ford et al., 2015; O'Brien et al., 2014) have been put forward to reconcile the observed discrepancies between Mg/Ca and TEX_{86}, which will be assessed here in light of the additional evidence from Δ_{47}.

4.3. Hypothesis 1: Decreasing IPWP Mixed Layer Temperatures

If the TEX_{86} records are interpreted as reliable evidence for a long-term cooling of surface waters in the IPWP since the Pliocene, then the other two proxies (Mg/Ca and Δ_{47}) must have been influenced by secondary processes in addition to temperature. These secondary influences would need to bias temperature toward increasingly colder values downhole to mask the long-term trend indicated by the TEX_{86} data.

As discussed above, possible influencing factors on the Mg/Ca signal include changes in dissolution processes preferentially removing Mg-rich calcite (e.g., Brown & Elderfield, 1996; Reuning et al., 2005; Rosenthal & Lohmann, 2002), and changes in Mg/Ca_{sw} (see Evans et al., 2016; O'Brien et al., 2014). If not accounted for, both might bias Pliocene Mg/Ca toward colder temperatures. Although some studies show that *T. sacculifer* (and thus *T. trilobus*) are not susceptible to selective dissolution (Brown & Elderfield, 1996; Sadekov et al., 2010), there is coretop evidence for a small effect related to dissolution in the IPWP (Dekens et al., 2002) at the depth of U1488. We have accounted for this effect by applying a small dissolution correction that is, kept constant over the time span covered by our record. This is because benthic foraminifera B/Ca data from ODP Site 806 in the IPWP indicates that $[CO_3^{2-}]$ did not change significantly over the last 5

Myrs (White & Ravelo, 2020) suggesting that there is no long-term change in dissolution that could mask a long-term cooling trend indicated by the TEX_{86} data.

Instead, in theory, Mg/Ca_{sw} could be masking the cooling trend. Since the Δ_{47} signal is independent of the seawater composition (Eiler, 2007; Ghosh et al., 2006), then its mismatch relative to the TEX_{86} trend must be related to a different process such as post-depositional diagenetic processes (Leutert et al., 2019). Both, the formation of secondary calcite on the surface of the foraminifera tests and the recrystallization of the biogenic structure at colder bottom or pore water conditions could alter the surface water Δ_{47} signal. In contrast, the Mg/Ca ratio of the samples may be preserved even when secondary calcification takes place within the sediment due to the possibility of closed system behavior if the recrystallization occurs within a small, enclosed volume (Kozdon et al., 2011). If anything, secondary calcite on the surface of foraminifera tests could alter the Mg/Ca-based temperature estimates toward warmer temperatures because inorganic calcite precipitated from pore water is enriched in Mg (Regenberg et al., 2007; Reuning et al., 2005; Rosenthal et al., 2000). If diagenetic overprinting were important for Site U1488, it would have resulted in a cold bias in Δ_{47}–based temperature estimates and either a warm bias or no effect in Mg/Ca-based temperature estimates. Assuming that diagenesis is the only process to have biased the data, we would expect a growing disagreement between Mg/Ca and Δ_{47} temperatures, which is not observed. This means that different processes are needed to explain the lack of cooling seen in Mg/Ca and Δ_{47}, and these would need to coincidently influence the two proxies at the same time, in the same direction and to roughly the same extent in order to explain the observed agreement between the two proxies. Thus, for hypothesis 1 to be true, the Mg/Ca record could be affected by changing Mg/Ca_{sw} (O'Brien et al., 2014), as discussed above, while Δ_{47} could be biased by diagenetic overprinting increasing downhole.

4.3.1. Preservation of *T. Trilobus* Across Time Intervals

Although initial shipboard analysis did not reveal any evidence for substantial diagenetic alteration over the last 5.6 Myrs at Site U1488, this initial preservation study was performed on relatively few samples, mostly outside the time intervals selected for this study. Therefore, we evaluated the possibility of increasing diagenetic effects on the Δ_{47} signal downhole by analyzing individual specimens of *T. trilobus* from all time intervals under the SEM (Figure 5). For each interval, we looked for signs of dissolution and secondary precipitation on the outer (Figures 5b1–5b8) and inner (Figures 5c1–5c8) surface of the chambers and for evidence of recrystallization in cross sections of broken chambers (Figures 5d1–5d8).

The majority of samples are characterized by very good preservation. The youngest (Holocene) sample from the first time interval (Figures 5a1–5d1) can be used as an example for a pristine looking specimen. The surface texture outside and inside is smooth (Figures 5b1 and 5c1) and typical features such as pores and spine holes are clearly visible and well preserved (Figure 5b1). Wall cross sections (Figure 5d1) reveal a microcrystalline structure that suggests biogenic calcite with little alteration. Furthermore, neither this sample nor any of the other samples analyzed contained substantial amounts of infillings with unconsolidated sediment. The 0.93 Ma old sample reveals the same preservation state as the surface (Figure 5a2–5d2). At 1.8 and 2.5 Ma, first signs of secondary calcite in the form of a very thin (~1 μm) layer of angular crystals can be identified on the surface of the foraminifera tests (Figures 5a3–5d4). Additionally, Figure 5a4 shows minimal evidence for dissolution in the form of slightly more rounded surface structures. However, these alterations of the foraminifera are most likely negligible with respect to their influence on test geochemistry. At 3.2 Ma the layer of secondary calcite on the surface is more pronounced, potentially allowing for a detectable effect on the geochemistry (Figures 5a5–5d5). In contrast, samples at 4.1 and 5.1 Ma (Figures 5a6–5d7) are characterized by only minor amounts of secondary calcite, minor evidence for dissolution and generally good preservation comparable to the younger samples <3 Ma. These observations suggests that effects of diagenesis on samples at this site are variable within the sediment and do not steadily increase downhole. The oldest time interval analyzed in this study (5.6 Ma) reveals the strongest evidence for diagenetic effects (Figures 5a8–5d8): The outside and inside of the calcite test are covered with a crust of inorganic secondary calcite.

Overall, there were no signs of recrystallization on scales observable with our analysis (Figure 5d1–5d8), minor evidence for dissolution (Figure 5b1–5d8) and variable amounts of secondary calcite growth found on the surface of the foraminifera tests (Figure 5b1–5c8). We note that we cannot rule out recrystallization at sub-micron scales. However, based on the evidence obtained, it seems unlikely that preservation

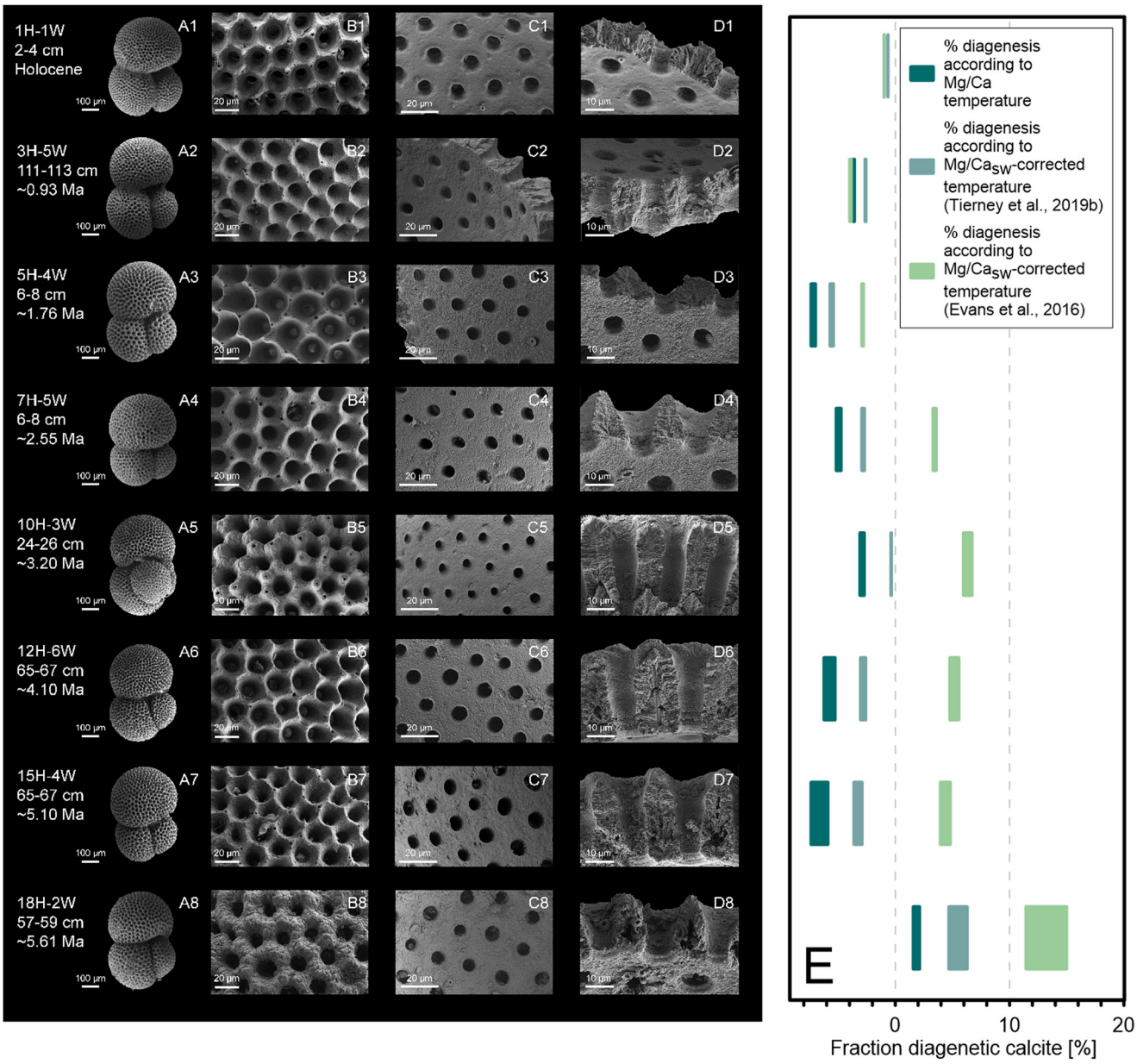

Figure 5. SEM pictures used to determine the preservation of *T. trilobus* across all time intervals (A-D) and the fraction of diagenetic calcite (E) needed to explain the temperature difference between the Δ_{47} and Mg/Ca records. A1-A8: Intact specimens of *T. trilobus* prior to cleaning. B1-D8: Detailed images of the outer and inner surface (B1-B8 and C1-C8, respectively) as well as wall cross sections (D1-D8) used to access the preservation state. E: Fraction of diagenetic calcite calculated using benthic Mg/Ca (Lear et al., 2015) for bottom-water temperatures and assuming that the Mg/Ca-based temperatures using Gray and Evans (2019) without (dark green) and with the Mg/Ca$_{sw}$ correction proposed by Evans et al. (2016) (light green) or Tierney, Malevich, et al. (2019) (teal) represent true mixed layer temperature. The width of the green shaded areas represent the range between the two endmember scenarios that the diagenetic fraction was either formed at the bottom water-sediment interface or at the final burial depth within the sediment.

deteriorated downhole in a consistent way to an extent that would substantially affect the proxy data. Instead, two intervals revealed evidence for considerable secondary calcite (samples at 3.2 and 5.6 Ma) that may be detectable in the geochemical proxy data, with the oldest interval being most severely affected by calcite overgrowth. All other samples show only very minor signs of alteration.

4.3.2. Diagenetic Effects on the Δ_{47} Signal

Based on the SEM images presented (Figures 5a–5d) some minor effect of diagenetic alteration, namely secondary calcite precipitated at bottom water or pore water temperature, cannot be ruled out. We used a

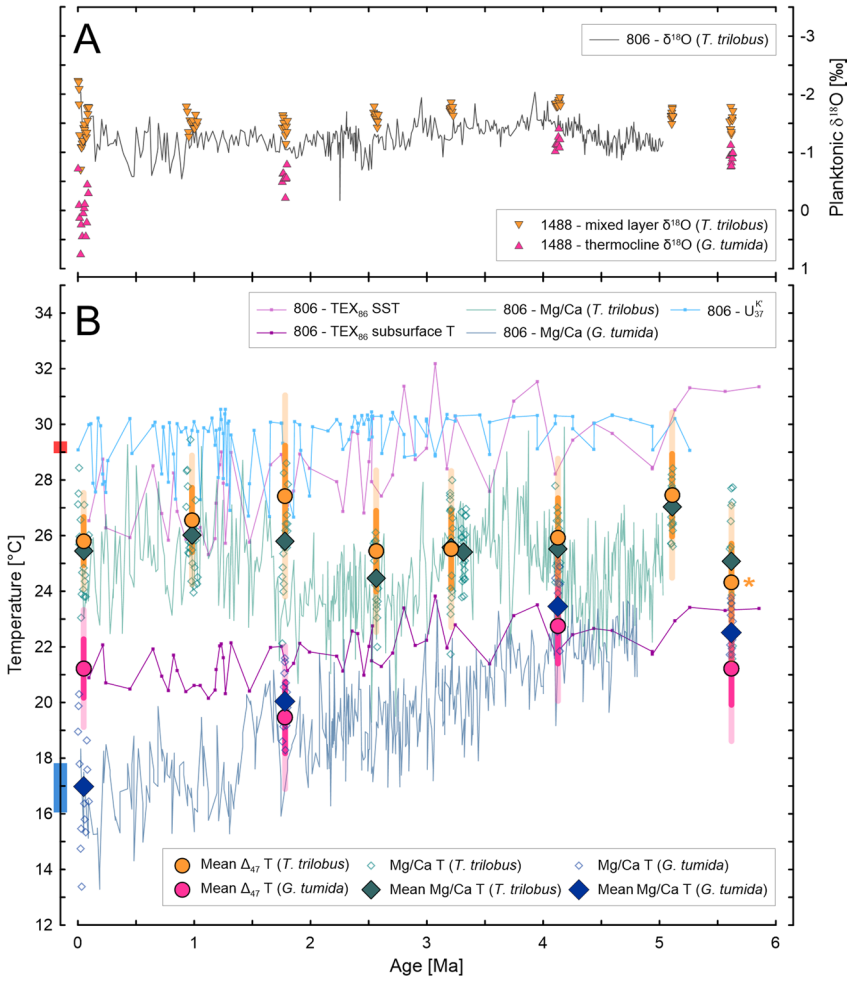

Figure 6. Multi-proxy data from Site U1488 across the last 5.6 Myrs compared to other records from the IPWP. (a) Mixed layer *T. trilobus* (orange triangles) and thermocline *G. tumida* (magenta triangles) $\delta^{18}O$ shown against the mixed layer $\delta^{18}O$ record from Site 806 (black line, Wara et al., 2005). (b) Mixed layer (*T. trilobus*) and thermocline (*G. tumida*) Mg/Ca (green and dark blue diamonds, respectively) and Δ_{47} temperatures (orange and magenta filled circles, respectively) compared to temperature records from Site 806: $U^{K'}_{37}$-derived sea surface temperatures (light blue line, Etourneau et al., 2010; Pagani et al., 2010; Zhang et al., 2014) were recalculated by Tierney, Haywood, et al. (2019). Mg/Ca mixed layer (*T. trilobus*, gray line, Wara et al., 2005) and thermocline temperatures (*G. tumida*, blue line, Ford et al., 2015) were recalculated using the same methodological approach as our U1488 records: The calibration by Gray and Evans (2019) and Anand et al. (2003) were used for *T. trilobus* and *G. tumida*, respectively. Both species were corrected for moderate Mg/Ca_{sw} changes using the Mg/Ca_{sw} correction from Tierney, Malevich, et al. (2019). TEX_{86}-based temperatures (Zhang et al., 2014) were recalculated using both a bayesian SST calibration (light purple, Tierney & Tingley, 2015) and a 0–200 m subsurface calibration (dark purple, Kim et al.,2012). Filled symbols represent average values for the time intervals while open symbols show the Mg/Ca temperatures of individual samples within each time interval. Red and blue bars on the left highlight the seasonal range of modern-day water temperatures at 0 and 200 m, respectively, according to Locarnini et al. (2010). Error bars for the Δ_{47} values represent 68% and 95% confidence intervals. The orange asterisk highlights the clumped isotope value potentially affected by a significant amount of diagenetic secondary calcite. Note that all foraminifera-based data from Site 806 were plotted using the age model used in Ford et al. (2015) while TEX_{86} and $U^{K'}_{37}$ data was kept on the original age models from the respective publications (see Zhang et al., 2014 and Tierney, Haywood, et al., 2019, respectively).

linear mixing model (see Material and Methods) to visualize the amounts of diagenetic calcite that would be able to cause the observed discrepancy between Δ_{47} and the Mg/Ca temperatures corrected for the different proposed Mg/Ca_{sw} changes (based on Evans et al. (2016) and Tierney, Malevich, et al. (2019)). The calculated fractions of secondary calcite serve as an illustration for the potential influence of diagenesis on the Δ_{47} data, but should not be taken at face value. Our diagenesis model is a simplified approximation of

the actual processes and does not include any uncertainties in the underlying Mg/Ca and Δ_{47} data. Note that the Mg/Ca_{sw} changes proposed by Evans et al. (2016) are based on the assumption that the trends in TEX_{86} temperature are correct, and thus the resulting estimates of diagenetic calcite are designed to provide a good match between the Δ_{47} and TEX_{86} data. For comparison, we did the same calculation without applying any Mg/Ca_{sw} correction.

Values calculated for the fraction of diagenetic calcite (Figure 5e) range between −4% and 15% when correcting for the Mg/Ca_{sw} changes suggested by Evans et al. (2016) and −6% and 6% using the Mg/Ca_{sw} correction by Tierney, Malevich, et al. (2019). The diagenetic fractions range from −7 to +2% when using the uncorrected Mg/Ca values. Negative percentages are a consequence of mean clumped isotope temperatures being slightly warmer than Mg/Ca temperatures, likely due to analytical uncertainty and potentially slightly underestimated dissolution effects on the Mg/Ca data. This apparent systematic bias may lead to negative percentages wherever no significant amount of diagenetic calcite is present.

Our diagenesis estimates indicate the highest amounts of diagenetic calcite (7% and 15% using Evans et al. (2016) for the Mg/Ca_{sw} correction) for the same two intervals (3.2 and 5.6 Ma, respectively) that revealed some degree of diagenetic overprint by secondary precipitation of inorganic calcite in the SEM images (Figures 5a5 and 5a8), suggesting that diagenetic alteration can explain small differences between the proxies. The Mg/Ca data corrected using Mg/Ca_{sw} from Tierney, Malevich, et al. (2019) only indicates a significant diagenetic fraction >5% for the oldest time interval. The gradual downhole increase of diagenetic alteration required to bring Δ_{47} temperatures into agreement with Mg/Ca when using the Mg/Ca_{sw} correction by Evans et al. (2016) (Figure 5e, light green symbols) and thus with the TEX_{86} records is not supported by the SEM-based preservation analysis. The observation that foraminifera in several of the older samples look just as pristine as those from the younger ones, while the visible calcite overgrowth detected in two of the time intervals coincides with higher calculated percentages of diagenetic calcite in Figure 5e, and thus slightly larger discrepancies between the proxies, argues against a gradual accretion of diagenetic effects at this site masking a continuous warming trend.

4.3.3. Changes in Foraminifera Ecology

Another possibility could be that a process that specifically affects foraminifera masks a long-term cooling trend in both Mg/Ca and Δ_{47}. This could for example, be a long-term change in habitat depth from deeper water depths (colder temperatures) in the Pliocene to shallower depths later in the record, or a change in growing season. We cannot fully exclude this possibility, but three arguments speak against it explaining the discrepancy between foraminifera- and TEX_{86}-based estimates: First, in the IPWP, *T. trilobus* already today appears to occupy a comparatively deep habitat for this species (see Section 2.2), making an even deeper habitat in the Pliocene little plausible. Second, seasonal temperature variability in the tropical waters of the IPWP is small today and does not appear to have changed significantly since the Pliocene, based on single foraminifera analysis at Site 806 (Ford & Ravelo, 2019). Furthermore, alkenone-based sea surface temperatures, although hampered by being close to the upper temperature limit of this method, agree better with the lack of a substantial long-term trend suggested by the foraminifera proxies than with the trend suggested by TEX_{86} (Figure 6b).

4.4. Hypothesis 2: No Long-Term Trend in IPWP Mixed Layer Temperatures

Taken at face value, the mixed layer temperatures from Mg/Ca and Δ_{47} suggest some variations in mixed layer temperature over time, but no clear overall trend in the long-term evolution of central warm pool mixed layer temperatures. This result is made more robust by the nature of our analytical approach, which focuses on mean temperatures for whole glacial-interglacial cycles. This strategy introduces a cold bias on the two youngest time intervals (100 kyr-world) where glacial periods are longer than interglacials. Figure 3c shows that average temperatures reconstructed for the whole interval from Mg/Ca and Δ_{47} are closer to the LGM value than to the Holocene. Mg/Ca-based mixed layer temperatures at Site 806 (Wara et al., 2005), recalculated using the same methodological procedure used in our study (calibration by Gray and Evans (2019) and correction for Mg/Ca_{sw} changes suggested by Tierney, Malevich, et al. (2019)), suggest the same temporal pattern as mixed layer temperatures at Site U1488 (Figure 6b). Good agreement between the two sites is also observed in the foraminifera $\delta^{18}O$ data (Wara et al., 2005, Figure 6a), indicating that the two sites located

in the central warm pool were influenced by similar environmental conditions and processes over the last 5.6 Myrs.

The lack of an overall trend toward higher maximum mixed layer temperatures during the Pliocene is in agreement with the $U^{K'}_{37}$ record from Site 806 (Etourneau et al., 2010; Pagani et al., 2010; Zhang et al., 2014; recalculated by Tierney, Haywood, et al., 2019, Figure 6b), interpreted as SST signal. The slight cooling trend visible in this data set (Tierney, Haywood, et al., 2019) is mainly driven by a growing amplitude between cooler minimum temperatures after the Pliocene while maximum temperatures are relatively consistent across the last 5.3 Myrs. While the $U^{K'}_{37}$-based temperatures are hampered by large uncertainty because they are close to the upper limit of this temperature proxy, they do not suggest the same temporal pattern as the foraminifera proxies. The apparant variations in the temperature difference between foraminifera proxies and alkenones could suggest temperature changes slightly below the sea surface (recorded by *T. trilobus*), temporal changes in the preferred habitat depth of *T. trilobus*, or changes in the season recorded by either proxy. These variations warrant further investigation, but do not confound the overall observation that none of these proxies show cooling to the same extent as TEX_{86}.

If the Mg/Ca and Δ_{47} records are taken as evidence that warm pool mixed layer temperatures over the last ~5 Myrs lack a substantial long-term trend, other influences besides surface temperature must have influenced the TEX_{86} signal. It has previously been suggested that TEX_{86} data might not reflect a pure surface temperature signal, but are also influenced by subsurface temperatures down to 200 m or even integrate over a larger part of the water column down to 1,000 m (reviewed in Zhang & Liu, 2018).

Ford et al. (2015) suggested that TEX_{86} data from the IPWP reflects thermocline cooling based on an observed Mg/Ca trend in the subsurface species *G. tumida* from Site 806 (Figure 6b). While derived for four time intervals only, our Mg/Ca-based temperature reconstructions for *G. tumida* agree with the Site 806 Mg/Ca data. The thermocline temperatures reconstructed from Mg/Ca on *G. tumida* (calibration by Anand et al. (2003) and Mg/Ca_{sw} correction by Tierney, Malevich, et al. (2019), implemented as described in section 4.1) at Sites U1488 and 806 both suggest warmer Late Miocene and Pliocene temperatures (22°C–23°C) followed by a cooling trend to ~17°C in the youngest interval at Site U1488 and similar temperatures at Site 806 (Figure 6b). We note that the magnitude of the thermocline cooling reconstructed with *G. tumida* is associated with some uncertainty due to the lack of constraints on the sensitivity of Mg/Ca in this species to Mg/Ca_{sw} changes (see Section 4.1). In the hypothetical, extreme case of zero sensitivity (i.e., no influence of Mg/Ca_{sw} on the signal), the cooling would be about 0.5°C less than shown in Figure 6b. Either way, the pattern in *G. tumida* Mg/Ca resembles the trend from lighter to heavier $\delta^{18}O$ values from the same species at Site U1488 (Figure 6a), which results in a long-term increase in the $\delta^{18}O$ offset between *T. trilobus* and *G. tumida*.

The Δ_{47} temperatures reconstructed for *G. tumida* agree, within error, with the Mg/Ca-based temperatures for the oldest three of our four time intervals. Generally, mean Δ_{47} temperatures are slightly (1°C–2°C) colder in these intervals, which might indicate that the multi-species calibration used for Mg/Ca from *G. tumida* has a systematic offset from the Δ_{47} calibration. The youngest time interval, however, does not fit this general pattern. The Δ_{47} data for this interval suggest a temperature of >20°C which is significantly warmer than the Mg/Ca-based temperature. Moreover, the youngest Δ_{47} temperature is also in disagreement with the long-term trend seen in the $\delta^{18}O$ data derived from the same measurements (see Figure 6a). We currently do not have an explanation for this discrepancy between Δ_{47} and Mg/Ca (and $\delta^{18}O$) in the youngest time interval, which will need to be further investigated by increasing the data density for Δ_{47}. However, based on the agreement between patterns visible in the Mg/Ca and $\delta^{18}O$ data across the entire *G. tumida* record, we interpret the Δ_{47}-based thermocline temperature for the youngest time interval to be too warm. Despite the apparent discrepancy we note that temperature estimates from both proxies for the youngest interval are within the wide temperature range for the expected thermocline habitat of *G. tumida* (145–273 m, ~12–22°C, Farmer et al., 2007; Cléroux et al., 2013), and the temperature uncertainty ranges from Mg/Ca and Δ_{47} overlap.

In summary, our coupled Mg/Ca and Δ_{47} measurements indicate that mixed layer temperatures determined from *T. trilobus* in the central warm pool fluctuated, but they do not appear to have cooled substantially and systematically from the Pliocene to recent, similar to the pattern previously observed for Site 806 based on

Mg/Ca (Wara et al., 2005). In the thermocline, in contrast, taking the more precise Mg/Ca measurements for *G. tumida* at face value, there is a long-term cooling trend by several degrees between 4 Ma and today both at Sites 806 and U1488. This interpretation is also supported by the observation that the mixed layer (*T. trilobus*) and thermocline (*G. tumida*) $\delta^{18}O$ records diverge over time with the thermocline data becoming more positive from the Pliocene to today (Figure 6a). In light of these findings, the observed trend in the TEX_{86} data could reflect the long-term thermocline cooling, as suggested by Ford et al. (2015). Recently, Zhang and Liu (2018) investigated the depth range the TEX_{86} signal is integrating over. Although the authors argue against a deep (several hundred meters) origin, they conclude that TEX_{86} may be influenced by subsurface temperatures down to 200 m. At Site U1488, the top of the thermocline sits well above this water depth (Locarnini et al., 2010) making a thermocline influence on the TEX_{86} signal a likely explanation for the apparent proxy discrepancies. This interpretation is in agreement with several studies proposing a contribution of subsurface production of the GDGT signal influencing TEX_{86}-based temperature reconstructions (Ho & Laepple, 2016; Kim et al., 2012; Tierney & Tingley, 2015; Richey & Tierney, 2016; Zhang & Liu, 2018). Applying a shallow subsurface (0–200 m) temperature calibration calculated by Kim et al. (2012) for the Pacific Ocean to the TEX_{86} record from Site 806 yields temperatures in between the mixed layer record from *T. trilobus* and thermocline temperatures calculated from *G. tumida* (Figure 6). Furthermore, the long-term cooling trend of ~5°C (25°C–~20°C) resembles the *G. tumida* record. Therefore, the absolute temperatures and cooling trend are in accordance with the interpretation that the TEX_{86} signal integrates temperature across the upper 200 m of the water column. The TEX_{86} SST calibration from Tierney and Tingley (2015) on the other hand reveals temperatures in line with the $U^{K'}_{37}$ data (Tierney, Haywood, et al., 2019) for the Pliocene but diverges from this SST record during the Pleistocene. Additional TEX_{86} calibrations are shown in the Supplementary Material (Figures S1–S3).

Based on the sum of evidence presented above, we interpret Mg/Ca and Δ_{47} measured in *T. trilobus* to represent accurate mixed layer temperatures. A minor correction for past Mg/Ca_{sw} changes seems sufficient to bring Mg/Ca and Δ_{47} temperatures into agreement for the last ~5 Myrs. This is consistent with the compilation of past Mg/Ca_{sw} changes by Tierney, Malevich, et al. (2019), which suggests only moderate changes during the Plio-Pleistocene. The smoothed fit through this compilation of datasets agrees well with data from calcite veigns (Coggon et al., 2010) but indicates smaller Mg/Ca_{sw} changes than for example, suggested by halite-based reconstructions (Brennan et al., 2013; Horita et al., 2002; Lowenstein et al., 2001). Applying this correction to our Mg/Ca record leads to temperatures still in good agreement with the independent Δ_{47} proxy (Figure 4).

4.5. Implications for Plio-Pleistocene Climate

Temperatures in the IPWP have been identified as an important driver of tropical and subtropical hydroclimate through heat and moisture advection (Burls et al., 2017). Our study uses multi-proxy data to determine IPWP temperatures during the Plio-Pleistocene with important implications for climate dynamics in this region and beyond.

First, our data agrees well with the foraminifera-based (Wara et al., 2005) and $U^{K'}_{37}$-derived temperature records (Etourneau et al., 2010; Pagani et al., 2010; Zhang et al., 2014; recalculated by Tierney, Haywood, et al., 2019) from Site 806 on the Ontong Java Plateau indicating that the observed pattern of relatively stable surface ocean temperatures is representative for the central IPWP. A recent compilation of temperature records for a short interval in the middle Pliocene Warm Period (KM5c; McClymont et al., 2020) suggests only slightly warmer temperatures for the warm pool (1°C–2°C) compared to the pre-industrial state, and note good agreement with PlioMIP2 model results (Hunter et al., 2019; Samakinwa et al., 2020), which also indicate that the IPWP was 1°C–2°C warmer. As that PlioVar compilation and PlioMIP2 targeted a very specific, short, and especially warm interval in the Pliocene, their results may not be directly comparable with our interval approach. The slightly warmer temperatures found in that particular interval appear, however, to be consistent with our findings, which represent longer time-averaged conditions that also contain cooler climate states. The intriguing million-year scale temperature pattern first observed by Wara et al. (2005) and now strongly supported by our data warrants further investigation as it might suggest variations in surface temperatures or in the thermal structure of the upper water column (given that $U^{K'}_{37}$ does not show the same variability).

Second, our data has implications for reconstructing zonal and meridional gradients in that it suggests that at most a minor Mg/Ca_{sw} correction (Tierney, Malevich, et al., 2019) is required to correct for Pliocene seawater changes when interpreting Mg/Ca records in other tropical and extratropical regions. Combined with other records from the tropical and subtropical Pacific (Brierley et al., 2009; Wara et al., 2005), our data is in accordance with reduced meridional and zonal temperature gradients during the Early Pliocene. This Pacific mean state could have caused the water content of the atmosphere to increase due to warmer sea surface temperatures in the east, and the large-scale atmospheric Hadley Circulation to be weaker during the Early Pliocene thus shifting global precipitation patterns and cloud cover (Brierley et al., 2009; Burls & Fedorov, 2017). These atmospheric changes induced by tropical sea surface temperature patterns could have had major implications for regional and global climate: Both climate models and data from the Pliocene indicate that wetter than modern conditions prevailed in parts of Africa, Australia (Brierley et al., 2009), North America (Goldner et al., 2011), and the subtropical west Pacific (Burls & Fedorov, 2017). Globally, the increase of the atmospheric water content has been proposed as an important factor sustaining a warm climate during the Pliocene by changing the net radiative forcing (Brierley et al., 2009). Moreover, variations in cloud cover, which has been identified as an important feedback mechanism influencing climate sensitivity (Haugstad et al., 2017; Rugenstein et al., 2016), may have played an additional role in changing the radiative budget of the atmosphere during the Pliocene (Brierley et al., 2009; Burls & Fedorov, 2014). In addition, climate models suggest that the Pliocene ocean temperature patterns characterized by reduced SST gradients could influence stratification in the subtropical North Pacific and allow for the establishment of meridional overturning in the Pacific Ocean (Burls et al., 2017).

Third, the evidence for a Plio-Pleistocene cooling of the thermocline in the tropical West Pacific presented in this study, although based on sparse data, supports the long-term ~4°C thermocline cooling trend from the Early Pliocene to the late Holocene described at nearby Site 806 (Ford et al., 2015). The cooling/shoaling of thermocline waters across the equatorial Pacific has been related to the establishment of the modern-day east Pacific cold tongue. This cooling in the eastern equatorial Pacific may have, in turn, been an important factor for the onset of the Northern Hemisphere glaciation through a cooling influence on North America (Huybers & Molnar, 2007) and Plio-Pleistocene global cooling in general (Ford et al., 2015).

5. Summary

We used paired Mg/Ca and Δ_{47} analysis on two species of planktonic foraminifera at IODP Site U1488 to reconstruct the Plio-Pleistocene mixed layer and thermocline temperature evolution of the IPWP. The combination of two independent proxies measured on the same samples and foraminifera species allowed us to investigate the effect of potential secondary influences such as past Mg/Ca_{sw} changes and diagenetic alteration on the individual methods. Furthermore, our combined record sheds light on the previously observed mismatch between Plio-Pleistocene Mg/Ca and TEX_{86} temperature reconstructions in this region.

Before taking possible changes in Mg/Ca_{sw} into account, neither our Mg/Ca record nor the Δ_{47} mixed layer temperature reconstructions support the long-term cooling hypothesis derived from several TEX_{86} records generated in this region (O'Brien et al., 2014; Zhang et al., 2014). While the absence of a cooling trend in the mixed layer Mg/Ca signal alone has previously been explained by long-term Mg/Ca_{sw} changes, our Δ_{47} record argues against this idea. Since Δ_{47} is insensitive to past ocean chemistry changes, an additional, independent process such as diagenetic alteration would be needed to explain the similarity between the Mg/Ca and the Δ_{47} signal. This process would need to bias the Δ_{47} data in the same direction and to the same degree as the proposed Mg/Ca_{sw} change would bias the Mg/Ca record. As shown by the linear mixing model we used to quantify the potential diagenetic influence on Δ_{47}, a gradual downhole increase of the diagenetic overprint on the Δ_{47} values would be needed to explain the temperature difference between Δ_{47} and the TEX_{86} records. Although small amounts of recrystallization could have escaped detection, a gradual increase of diagenetic overprinting does not seem to be supported by the SEM images, where instead samples from 4.1 and 5.1 Ma appear better preserved compared to samples from 3.3 Ma. The Δ_{47} and Mg/Ca-based estimates furthermore suggest a similar pattern of variability over the interval studied here, which also seems less likely to obtain if the proxies were influenced by different additional, non-thermal processes.

We cannot rule out that some extent of Plio-Pleistocene cooling was masked by past Mg/Ca_{sw} changes of the magnitude suggested by Tierney, Malevich, et al. (2019) and by the analytical uncertainty of the Δ_{47} measurement in combination with the effects of minor diagenetic alterations. However, the scale of cooling suggested by TEX_{86} records from the region (O'Brien et al., 2014; Zhang et al., 2014) does not seem to be supported by the sum of the evidence available to us. Instead, the *T. trilobus* Mg/Ca and Δ_{47} records are most likely a good representation of mixed layer (though not sea surface) temperatures in this region.

In contrast, the *G. tumida* Mg/Ca records from both Site U1488 and 806 (Ford et al., 2015) provide evidence for a long-term thermocline cooling from ~4 Ma to present. As proposed earlier (Ford et al., 2015), this subsurface trend could be an explanation for the cooling visible in the TEX_{86} records from this region if that proxy was not only recording SSTs but instead integrating surface and shallow subsurface (<200 m) temperatures as suggested by a number of studies (e.g., Hurley et al., 2018; Tierney & Tingley, 2015; Zhang & Liu, 2018). By applying calibrations that allow reconstructing in situ temperatures instead of SSTs, a consistent pattern of changes in the thermal structure of the water column appears to emerge.

If correct, the minor change in Mg/Ca_{sw} across the last ~5 Myrs suggested by our data and the absence of long-term mixed layer cooling in the IPWP across this time interval also substantiates the interpretation of other Mg/Ca records from the equatorial Pacific. In combination with Mg/Ca-based reconstructions from the Eastern Equatorial Pacific, our findings support a previously suggested weaker zonal temperature gradient during the Early Pliocene (Ford et al., 2015; Wara et al., 2005).

Data Availability Statement

The trace metal and isotope data of this study are available at Pangaea (https://doi.org/10.1594/PANGAEA.933340). The raw replicate level isotope data are available at EarthChem (https://doi.org/10.26022/IEDA/111920).

Acknowledgments
The authors are thankful to Jessica Tierney and the two anonymous reviewers for their constructive comments and suggestions. The authors thank the International Ocean Discovery Program (IODP) for the sample material provided for this study. The authors would also like to acknowledge the Shipboard Scientific party of IODP Expedition 363 for their work in gathering and describing the cores. The authors thank Eivind W. N. Støren for access to the facilities of EARTHLAB and Ulrike Proske and Jordan Donn Holl for their contribution to the sample preparation. The authors are grateful to Allegra Liltved, Sze Ling Ho and Raúl Iván Tapia Arroyo for their help during the clumped isotope analysis and to Enver Alagoz, Pål Tore Mørkved, and the clumped isotope group at the University of Bergen for laboratory assistance and technical support. Funding for clumped isotope analysis was provided by the Trond Mohn Foundation and the European Research Council (ERC) under the European Union's Horizon 2020 research and innovation program (grant agreement No 638467). Clumped isotope analyses were performed at the Norwegian national infrastructure laboratory FARLAB (RCN project 245907). The authors thank Michelle Drake and Sarah White for their data analysis expertize and Rob Franks and Brian Dreyer at the Marine Analytical Lab at UCSC for aid in ICP-OES analysis. Funding for Mg/Ca analysis was provided by the U.S. National Science Foundation OCE-1736686 (ACR).

References

Anand, P., Elderfield, H., & Conte, M. H. (2003). Calibration of Mg/Ca thermometry in planktonic foraminifera from a sediment trap time series. *Paleoceanography*, *18*. https://doi.org/10.1029/2002PA000846

André, A., Weiner, A., Quillévéré, F., Aurahs, R., Morard, R., & Douady, C. J. (2013). The cryptic and the apparent reversed: Lack of genetic differentiation within the morphologically diverse plexus of the planktonic foraminifer Globigerinoides sacculifer. *Paleobiology*, *39*(01), 21–39. https://doi.org/10.1666/0094-8373-39.1.21

Bé, A., & Tolderlund, D. (1971). Distribution and ecology of living planktonic foraminifera in surface waters of the Atlantic and Indian Oceans. *Paper presented at the The Micropalaeontology of Oceans: Proceedings of the Symposium Held in Cambridge from 10 to 17 September 1967 Under the Title 'Micropalaeontology of Marine Bottom Sediments'*.

Bemis, B. E., Spero, H. J., Bijma, J., & Lea, D. W. (1998). Reevaluation of the oxygen isotopic composition of planktonic foraminifera: Experimental results and revised paleotemperature equations. *Paleoceanography*, *13*(2), 150–160. https://doi.org/10.1029/98PA00070

Berger, W. H., Bonneau, M. C., & Parker, F. L. (1982). Foraminifera on the deep-sea floor - Lysocline and dissolution rate. *Oceanologica Acta*, *5*(2), 249–258. https://doi.org/10.1016/0198-0254(82)90178-9

Bernasconi, S. M., Daëron, M., Bergmann, K. D., Bonifacie, M., Meckler, A. N., Affek, H. P., et al. (2021). InterCarb: A community effort to improve interlaboratory standardization of the carbonate clumped isotope thermometer using carbonate standards. *Geochemistry, Geophysics, Geosystems*, *22*(5), e2020GC009588. https://doi.org/10.1029/2020GC009588

Bernasconi, S. M., Hu, B., Wacker, U., Fiebig, J., Breitenbach, S. F., & Rutz, T. (2013). Background effects on Faraday collectors in gas-source mass spectrometry and implications for clumped isotope measurements. *Rapid Communications in Mass Spectrometry*, *27*(5), 603–612. https://doi.org/10.1002/rcm.6490

Bernasconi, S. M., Müller, I. A., Bergmann, K. D., Breitenbach, S. F. M., Fernandez, A., Hodell, D. A., et al. (2018). Reducing uncertainties in carbonate clumped isotope analysis through consistent carbonate-based standardization. *Geochemistry, Geophysics, Geosystems*. https://doi.org/10.1029/2017gc007385

Bijma, J., & emleben, C. (1994). Population dynamics of the planktic foraminifer Globigerinoides sacculifer (Brady) from the central Red Sea. *Deep Sea Research Part I*, *41*(3), 485–510. https://doi.org/10.1016/0967-0637(94)90092-2

Brennan, S. T., Lowenstein, T. K., & Cendón, D. I. (2013). The major-ion composition of Cenozoic seawater: The past 36 million years from fluid inclusions in marine halite. *American Journal of Science*, *313*(8), 713–775. https://doi.org/10.2475/08.2013.01

Brierley, C. M., Fedorov, A. V., Liu, Z., Herbert, T. D., Lawrence, K. T., & LaRiviere, J. P. (2009). Greatly expanded tropical warm pool and weakened Hadley circulation in the Early Pliocene. *Science*, *323*(5922), 1714–1718. https://doi.org/10.1126/science.1167625

Brown, S. J., & Elderfield, H. (1996). Variations in Mg/Ca and Sr/Ca ratios of planktonic foraminifera caused by postdepositional dissolution: Evidence of shallow Mg-dependent dissolution. *Paleoceanography*, *11*(5), 543–551. https://doi.org/10.1029/96PA01491

Burke, K. D., Williams, J. W., Chandler, M. A., Haywood, A. M., Lunt, D. J., & Otto-Bliesner, B. L. (2018). Pliocene and Eocene provide best analogs for near-future climates. *Proceedings of the National Academy of Sciences*, *115*(52), 13288–13293. https://doi.org/10.1073/pnas.1809600115

Burls, N. J., & Fedorov, A. V. (2014). What controls the mean East–West sea surface temperature gradient in the Equatorial Pacific: The role of Cloud Albedo. *Journal of Climate*, *27*(7), 2757–2778. https://doi.org/10.1175/jcli-d-13-00255.1

Burls, N. J., & Fedorov, A. V. (2017). Wetter subtropics in a warmer world: Contrasting past and future hydrological cycles. *Proceedings of the National Academy of Sciences of the USA*, *114*(49), 12888–12893. https://doi.org/10.1073/pnas.1703421114

Burls, N. J., Fedorov, A. V., Sigman, D. M., Jaccard, S. L., Tiedemann, R., & Haug, G. H. (2017). Active Pacific meridional overturning circulation (PMOC) during the warm Pliocene. *Science Advances*, *3*. https://doi.org/10.1126/sciadv.1700156

Chaisson, W. P., & Ravelo, A. C. (2000). Pliocene development of the east-west hydrographic gradient in the equatorial Pacific. *Paleoceanography*, *15*(5), 497–505. https://doi.org/10.1029/1999pa000442

Cléroux, C., deMenocal, P., Arbuszewski, J., & Linsley, B. (2013). Reconstructing the upper water column thermal structure in the Atlantic Ocean. *Paleoceanography*, *28*(3), 503–516. https://doi.org/10.1002/palo.20050

Coggon, R. M., Teagle, D. A., Smith-Duque, C. E., Alt, J. C., & Cooper, M. J. (2010). Reconstructing past seawater Mg/Ca and Sr/Ca from mid-ocean ridge flank calcium carbonate veins. *Science*, *327*(5969), 1114–1117. https://doi.org/10.1126/science.1182252

Daëron, M., Blamart, D., Peral, M., & Affek, H. (2016). Absolute isotopic abundance ratios and the accuracy of Δ_{47} measurements. *Chemical Geology*, *442*, 83–96. https://doi.org/10.1016/j.chemgeo.2016.08.014

Defliese, W. F., & Lohmann, K. C. (2015). Non-linear mixing effects on mass-47 CO_2 clumped isotope thermometry: Patterns and implications. *Rapid Communications in Mass Spectrometry*, *29*(9), 901–909. https://doi.org/10.1002/rcm.7175

Dekens, P. S., Lea, D. W., Pak, D. K., & Spero, H. J. (2002). Core top calibration of Mg/Ca in tropical foraminifera: Refining paleotemperature estimation. *Geochemistry, Geophysics, Geosystems*, *3*(4), 1–29. https://doi.org/10.1029/2001GC000200

Dennis, K. J., Affek, H. P., Passey, B. H., Schrag, D. P., & Eiler, J. M. (2011). Defining an absolute reference frame for 'clumped' isotope studies of CO_2. *Geochimica et Cosmochimica Acta*, *75*(22), 7117–7131. https://doi.org/10.1016/j.gca.2011.09.025

Dowsett, H. J., Robinson, M. M., Haywood, A. M., Hill, D. J., Dolan, A. M., Stoll, D. K., et al. (2012). Assessing confidence in Pliocene sea surface temperatures to evaluate predictive models. *Nature Climate Change*, *2*(5), 365–371. https://doi.org/10.1038/nclimate1455

Drury, A. J., Weserhold, T., Ravelo, A. C., Kulhanek, D. K., Mountain, G., Holbourn, A., et al. (2021).Composite depth scale and splice revision for IODP Site U1488 using XRF core scanning data and composite core images. In A. E. Holbourn, D. K. Kulhanek, & the Expedition 363 Scientists (Eds.), *Western Pacific warm pool. Proceedings of the International Ocean Discovery Program, 363*. TX (International Ocean Discovery Program).

Dyez, K. A., & Ravelo, A. C. (2013). Late Pleistocene tropical Pacific temperature sensitivity to radiative greenhouse gas forcing. *Geology*, *41*(1), 23–26. https://doi.org/10.1130/g33425.1

Eiler, J. M. (2007). "Clumped-isotope" geochemistry—The study of naturally-occurring, multiply-substituted isotopologues. *Earth and Planetary Science Letters*, *262*(3–4), 309–327. https://doi.org/10.1016/j.epsl.2007.08.020

Eiler, J. M., & Schauble, E. (2004). $^{18}O^{13}C^{16}O$ in Earth's atmosphere. *Geochimica et Cosmochimica Acta*, *68*(23), 4767–4777. https://doi.org/10.1016/j.gca.2004.05.035

Emiliani, C. (1954). Depth habitats of some species of pelagic foraminifera as indicated by oxygen isotope ratios. *American Journal of Science*, *252*(3), 149–158. https://doi.org/10.2475/ajs.252.3.149

Erez, J., & Luz, B. (1983). Experimental paleotemperature equation for planktonic foraminifera. *Geochimica et Cosmochimica Acta*, *47*(6), 1025–1031. https://doi.org/10.1016/0016-7037(83)90232-6

Etourneau, J., Schneider, R., Blanz, T., & Martinez, P. (2010). Intensification of the Walker and Hadley atmospheric circulations during the Pliocene–Pleistocene climate transition. *Earth and Planetary Science Letters*, *297*(1), 103–110. https://doi.org/10.1016/j.epsl.2010.06.010

Evans, D., Brierley, C., Raymo, M. E., Erez, J., & Müller, W. (2016). Planktic foraminifera shell chemistry response to seawater chemistry: Pliocene–Pleistocene seawater Mg/Ca, temperature and sea level change. *Earth and Planetary Science Letters*, *438*, 139–148. https://doi.org/10.1016/j.epsl.2016.01.013

Evans, D., & Müller, W. (2012). Deep time foraminifera Mg/Ca paleothermometry: Nonlinear correction for secular change in seawater Mg/Ca. *Paleoceanography*, *27*(4). https://doi.org/10.1029/2012pa002315

Fantle, M. S., & DePaolo, D. J. (2006). Sr isotopes and pore fluid chemistry in carbonate sediment of the Ontong Java Plateau: Calcite recrystallization rates and evidence for a rapid rise in seawater Mg over the last 10 million years. *Geochimica et Cosmochimica Acta*, *70*(15), 3883–3904. https://doi.org/10.1016/j.gca.2006.06.009

Farmer, E. C., Kaplan, A., de Menocal, P. B., & Lynch-Stieglitz, J. (2007). Corroborating ecological depth preferences of planktonic foraminifera in the tropical Atlantic with the stable oxygen isotope ratios of core top specimens. *Paleoceanography*, *22*(3). https://doi.org/10.1029/2006PA001361

Fedorov, A. V., Brierley, C. M., & Emanuel, K. (2010). Tropical cyclones and permanent El Nino in the early Pliocene epoch. *Nature*, *463*(7284), 1066–1070. https://doi.org/10.1038/nature08831

Fedorov, A. V., Dekens, P. S., McCarthy, M., & Ravelo, A. C. (2006). The Pliocene Paradox (Mechanisms for a Permanent El Niño). *Science*, *312*(5779), 1485–1489. https://doi.org/10.1126/science.1122666

Ford, H. L., & Ravelo, A. C. (2019). Estimates of Pliocene Tropical Pacific temperature sensitivity to radiative greenhouse gas forcing. *Paleoceanography and Paleoclimatology*, *34*(1), 2–15. https://doi.org/10.1029/2018pa003461

Ford, H. L., Ravelo, A. C., Dekens, P. S., LaRiviere, J. P., & Wara, M. W. (2015). The evolution of the equatorial thermocline and the early Pliocene El Padre mean state. *Geophysical Research Letters*, *42*(12), 4878–4887. https://doi.org/10.1002/2015gl064215

Foster, G. L., Royer, D. L., & Lunt, D. J. (2017). Future climate forcing potentially without precedent in the last 420 million years. *Nature Communications*, *8*, 14845. https://doi.org/10.1038/ncomms14845

Ghosh, P., Adkins, J., Affek, H., Balta, B., Guo, W., Schauble, E. A., et al. (2006). ^{13}C–^{18}O bonds in carbonate minerals: A new kind of paleothermometer. *Geochimica et Cosmochimica Acta*, *70*(6), 1439–1456. https://doi.org/10.1016/j.gca.2005.11.014

Goldner, A., Huber, M., Diffenbaugh, N., & Caballero, R. (2011). Implications of the permanent El Niño teleconnection "blueprint" for past global and North American hydroclimatology. *Climate of the Past*, *7*(3), 723–743. https://doi.org/10.5194/cp-7-723-2011

Gothmann, A. M., Stolarski, J., Adkins, J. F., Schoene, B., Dennis, K. J., Schrag, D. P., et al. (2015). Fossil corals as an archive of secular variations in seawater chemistry since the Mesozoic. *Geochimica et Cosmochimica Acta*, *160*, 188–208. https://doi.org/10.1016/j.gca.2015.03.018

Grauel, A.-L., Schmid, T. W., Hu, B., Bergami, C., Capotondi, L., Zhou, L., & Bernasconi, S. M. (2013). Calibration and application of the 'clumped isotope' thermometer to foraminifera for high-resolution climate reconstructions. *Geochimica et Cosmochimica Acta*, *108*, 125–140. https://doi.org/10.1016/j.gca.2012.12.049

Gray, W. R., & Evans, D. (2019). Non-thermal influences on Mg/Ca in planktonic foraminifera: A review of culture studies and application to the last glacial maximum. *Paleoceanography and Paleoclimatology*, *34*, 306–315. https://doi.org/10.1029/2018pa003517

Haugstad, A. D., Armour, K. C., Battisti, D. S., & Rose, B. E. J. (2017). Relative roles of surface temperature and climate forcing patterns in the inconstancy of radiative feedbacks. *Geophysical Research Letters*, *44*(14), 7455–7463. https://doi.org/10.1002/2017gl074372

Haywood, A. M., Ridgwell, A., Lunt, D. J., Hill, D. J., Pound, M. J., Dowsett, H. J., et al. (2011). Are there pre-Quaternary geological analogues for a future greenhouse warming? *Philosophical Transactions of the Royal Society A: Mathematical, Physical & Engineering Sciences*, *369*(1938), 933–956. https://doi.org/10.1098/rsta.2010.0317

Hemleben, C., Spindler, M., Breitinger, I., & Deuser, W. G. (1985). Field and laboratory studies on the ontogeny and ecology of some globorotaliid species from the Sargasso Sea off Bermuda. *Journal of Foraminiferal Research*, *15*(4), 254–272. https://doi.org/10.2113/gsjfr.15.4.254

Hertzberg, J. E., Schmidt, M. W., Bianchi, T. S., Smith, R. W., Shields, M. R., & Marcantonio, F. (2016). Comparison of eastern tropical Pacific TEX_{86} and Globigerinoides ruber Mg/Ca derived sea surface temperatures: Insights from the Holocene and Last Glacial maximum. *Earth and Planetary Science Letters*, *434*, 320–332. https://doi.org/10.1016/j.epsl.2015.11.050

Ho, S. L., & Laepple, T. (2016). Flat meridional temperature gradient in the early Eocene in the subsurface rather than surface ocean. *Nature Geoscience*, *9*, 606. https://doi.org/10.1038/ngeo2763

Horita, J., Zimmermann, H., & Holland, H. D. (2002). Chemical evolution of seawater during the Phanerozoic: Implications from the record of marine evaporites. *Geochimica et Cosmochimica Acta*, *66*(21), 3733–3756. https://doi.org/10.1016/S0016-7037(01)00884-5

Hu, B., Radke, J., Schluter, H. J., Heine, F. T., Zhou, L., & Bernasconi, S. M. (2014). A modified procedure for gas-source isotope ratio mass spectrometry: The long-integration dual-inlet (LIDI) methodology and implications for clumped isotope measurements. *Rapid Communications in Mass Spectrometry*, *28*(13), 1413–1425. https://doi.org/10.1002/rcm.6909

Hunter, S. J., Haywood, A. M., Dolan, A. M., & Tindall, J. C. (2019). The HadCM3 contribution to PlioMIP phase 2. *Climate of the Past*, *15*(5), 1691–1713. https://doi.org/10.5194/cp-15-1691-2019

Hurley, S. J., Lipp, J. S., Close, H. G., Hinrichs, K.-U., & Pearson, A. (2018). Distribution and export of isoprenoid tetraether lipids in suspended particulate matter from the water column of the Western Atlantic Ocean. *Organic Geochemistry*, *116*, 90–102. https://doi.org/10.1016/j.orggeochem.2017.11.010

Huybers, P., & Molnar, P. (2007). Tropical cooling and the onset of North American glaciation. *Climate of the Past*, *3*(3), 549–557. https://doi.org/10.5194/cp-3-549-2007

Jansen, E., Mayer, L. A., Backman, J., Leckie, R. M., & Takayama, T. (1993). Evolution of Pliocene climate cyclicity at Hole 806B (5-2 Ma); oxygen isotope record. https://doi.org/10.2973/odp.proc.sr.130.028.1993

John, C. M., & Bowen, D. (2016). Community software for challenging isotope analysis: First applications of 'Easotope' to clumped isotopes. *Rapid Communications in Mass Spectrometry*, *30*(21), 2285–2300. https://doi.org/10.1002/rcm.7720

Kim, J.-H., Romero, O. E., Lohmann, G., Donner, B., Laepple, T., Haam, E., & Sinninghe Damsté, J. S. (2012). Pronounced subsurface cooling of North Atlantic waters off Northwest Africa during Dansgaard–Oeschger interstadials. *Earth and Planetary Science Letters*, *339–340*, 95–102. https://doi.org/10.1016/j.epsl.2012.05.018

Kim, J.-H., Schouten, S., Rodrigo-Gámiz, M., Rampen, S., Marino, G., Huguet, C., et al. (2015). Influence of deep-water derived isoprenoid tetraether lipids on the $TEX_{86}H$ paleothermometer in the Mediterranean Sea. *Geochimica et Cosmochimica Acta*, *150*, 125–141. https://doi.org/10.1016/j.gca.2014.11.017

Kim, S.-T., & O'Neil, J. R. (1997). Equilibrium and nonequilibrium oxygen isotope effects in synthetic carbonates. *Geochimica et Cosmochimica Acta*, *61*(16), 3461–3475. https://doi.org/10.1016/S0016-7037(97)00169-5

Kozdon, R., Kelly, D. C., Kita, N. T., Fournelle, J. H., & Valley, J. W. (2011). Planktonic foraminiferal oxygen isotope analysis by ion microprobe technique suggests warm tropical sea surface temperatures during the Early Paleogene. *Paleoceanography*, *26*(3). https://doi.org/10.1029/2010pa002056

Lear, C. H., Coxall, H. K., Foster, G. L., Lunt, D. J., Mawbey, E. M., Rosenthal, Y., et al. (2015). Neogene ice volume and ocean temperatures: Insights from infaunal foraminiferal Mg/Ca paleothermometry. *Paleoceanography*, *30*(11), 1437–1454. https://doi.org/10.1002/2015pa002833

LeGrande, A. N, & Schmidt, G. A. (2006). Global gridded data set of the oxygen isotopic composition in seawater. *Geophysical Research Letters*, *33*(12). https://doi.org/10.1029/2006gl026011

Leutert, T. J., Sexton, P. F., Tripati, A., Piasecki, A., Ho, S. L., & Meckler, A. N. (2019). Sensitivity of clumped isotope temperatures in fossil benthic and planktic foraminifera to diagenetic alteration. *Geochimica et Cosmochimica Acta*, *257*, 354–372. https://doi.org/10.1016/j.gca.2019.05.005

Liddy, H. M., Feakins, S. J., & Tierney, J. E. (2016). Cooling and drying in northeast Africa across the Pliocene. *Earth and Planetary Science Letters*, *449*, 430–438. https://doi.org/10.1016/j.epsl.2016.05.005

Lisiecki, L. E., & Raymo, M. E. (2005). A Pliocene-Pleistocene stack of 57 globally distributed benthic $\delta^{18}O$ records. *Paleoceanography*, *20*(1), https://doi.org/10.1029/2004pa001071

Locarnini, R., Mishonov, A., Antonov, J., Boyer, T., Garcia, H., Baranova, O. K., et al. (2010). World Ocean Atlas 2009. In Temperature, S. Levitus (Ed.), *NOAA Atlas NESDIS 68* (Vol. 1). US Government Printing Office.

Lohmann, G. P. (1995). A model for variation in the chemistry of planktonic foraminifera due to secondary calcification and selective dissolution. *Paleoceanography*, *10*(3), 445–457. https://doi.org/10.1029/95pa00059

Lowenstein, T. K., Timofeeff, M. N., Brennan, S. T., Hardie, L. A., & Demicco, R. V. (2001). Oscillations in Phanerozoic seawater chemistry: Evidence from fluid inclusions. *Science*, *294*(5544), 1086–1088. https://doi.org/10.1126/science.1064280

Martin, P. A., & Lea, D. W. (2002). A simple evaluation of cleaning procedures on fossil benthic foraminiferal Mg/Ca. *Geochemistry, Geophysics, Geosystems*, *3*(10), 1–8. https://doi.org/10.1029/2001GC000280

McClymont, E. L., Ford, H. L., Ho, S. L., Tindall, J. C., Haywood, A. M., Alonso-Garcia, M., et al. (2020). Lessons from a high CO_2 world: An ocean view from ~3 million years ago. *Climate of the Past Discussions*, *2020*, 1–27. https://doi.org/10.5194/cp-2019-161

McCorkle, D. C., Martin, P. A., Lea, D. W., & Klinkhammer, G. P. (1995). Evidence of a dissolution effect on benthic foraminiferal shell chemistry: $\delta^{13}C$, Cd/Ca, Ba/Ca, and Sr/Ca results from the Ontong Java Plateau. *Paleoceanography*, *10*(4), 699–714. https://doi.org/10.1029/95pa01427

Meckler, A. N., Ziegler, M., Millan, M. I., Breitenbach, S. F., & Bernasconi, S. M. (2014). Long-term performance of the Kiel carbonate device with a new correction scheme for clumped isotope measurements. *Rapid Communications in Mass Spectrometry*, *28*(15), 1705–1715. https://doi.org/10.1002/rcm.6949

Medina-Elizalde, M., & Lea, D. W. (2010). Late Pliocene equatorial Pacific. *Paleoceanography*, *25*(2). https://doi.org/10.1029/2009pa001780

Medina-Elizalde, M., Lea, D. W., & Fantle, M. S. (2008). Implications of seawater Mg/Ca variability for Plio-Pleistocene tropical climate reconstruction. *Earth and Planetary Science Letters*, *269*(3–4), 585–595. https://doi.org/10.1016/j.epsl.2008.03.014

Meinicke, N., Ho, S. L., Hannisdal, B., Nürnberg, D., Tripati, A., Schiebel, R., & Meckler, A. N. (2020). A robust calibration of the clumped isotopes to temperature relationship for foraminifers. *Geochimica et Cosmochimica Acta*, *270*, 160–183. https://doi.org/10.1016/j.gca.2019.11.022

Miller, K., Mountain, G., Wright, J., & Browning, J. (2011). A 180-million-year record of sea level and ice volume variations from continental margin and deep-sea isotopic records. *Oceanography*, *24*(2), 40–53. https://doi.org/10.5670/oceanog.2011.26

Molnar, P., & Cane, M. A. (2002). El Niño's tropical climate and teleconnections as a blueprint for pre-Ice Age climates. *Paleoceanography*, *17*(2), 11. https://doi.org/10.1029/2001pa000663

Mucci, A., & Morse, J. W. (1983). The incorporation of Mg^{2+} and Sr^{2+} into calcite overgrowths: Influences of growth rate and solution composition. *Geochimica et Cosmochimica Acta*, *47*(2), 217–233. https://doi.org/10.1016/0016-7037(83)90135-7

Müller, P. J., Kirst, G., Ruhland, G., von Storch, I., & Rosell-Melé, A. (1998). Calibration of the alkenone paleotemperature index U37K′ based on core-tops from the eastern South Atlantic and the global ocean (60°N–60°S). *Geochimica et Cosmochimica Acta*, *62*(10), 1757–1772. https://doi.org/10.1016/S0016-7037(98)00097-0

Neale, R., & Slingo, J. (2003). The maritime continent and its role in the global climate: A GCM study. *Journal of Climate*, *16*(5), 834–848. https://doi.org/10.1175/1520-0442(2003)016

O'Brien, C. L., Foster, G. L., Martínez-Botí, M. A., Abell, R., Rae, J. W. B., & Pancost, R. D. (2014). High sea surface temperatures in tropical warm pools during the Pliocene. *Nature Geoscience*, *7*(8), 606–611. https://doi.org/10.1038/ngeo2194

Pagani, M., Liu, Z., LaRiviere, J., & Ravelo, A. C. (2010). High Earth-system climate sensitivity determined from Pliocene carbon dioxide concentrations. *Nature Geoscience*, *3*(1), 27–30. https://doi.org/10.1038/ngeo724

Pearson, P. N. (2012). Oxygen isotopes in foraminifera: Overview and historical review. *Paleontological Society Papers*, *18*, 1–38. https://doi.org/10.1017/S1089332600002539

Peral, M., Daëron, M., Blamart, D., Bassinot, F., Dewilde, F., Smialkowski, N., et al. (2018). Updated calibration of the clumped isotope thermometer in planktonic and benthic foraminifera. *Geochimica et Cosmochimica Acta*. *239*, 1–16. https://doi.org/10.1016/j.gca.2018.07.016

Piasecki, A., Bernasconi, S. M., Grauel, A.-L., Hannisdal, B., Ho, S. L., Leutert, T. J., et al. (2019). Application of clumped isotope thermometry to benthic foraminifera. *Geochemistry, Geophysics, Geosystems*, *20*, 2082–2090. https://doi.org/10.1029/2018GC007961

Polik, C. A., Elling, F. J., & Pearson, A. (2018). Impacts of paleoecology on the TEX86 sea surface temperature proxy in the Pliocene-Pleistocene Mediterranean Sea. *Paleoceanography and Paleoclimatology*, *33*(12), 1472–1489. https://doi.org/10.1029/2018pa003494

Pujol, C., & Grazzini, C. V. (1995). Distribution patterns of live planktic foraminifers as related to regional hydrography and productive systems of the Mediterranean Sea. *Marine Micropaleontology*, *25*(2–3), 187–217. https://doi.org/10.1016/0377-8398(95)00002-I

Ravelo, A. C., Dekens, P. S., & McCarthy, M. (2006). Evidence for El Niño–like conditions during the Pliocene. *Geological Society of America Today*, *16*(3), 4. https://doi.org/10.1130/1052-5173(2006)016

Ravelo, A. C., & Fairbanks, R. G. (1992). Oxygen isotopic composition of multiple species of planktonic foraminifera: Recorders of the modern photic zone temperature gradient. *Paleoceanography*, *7*(6), 815–831. https://doi.org/10.1029/92PA02092

Ravelo, A. C., Fairbanks, R. G., & Philander, S. G. H. (1990). Reconstructing tropical Atlantic hydrography using planktontic foraminifera and an ocean model. *Paleoceanography*, *5*(3), 409–431. https://doi.org/10.1029/PA005i003p00409

Raymo, M. E., Kozdon, R., Evans, D., Lisiecki, L., & Ford, H. L. (2018). The accuracy of mid-Pliocene $\delta^{18}O$-based ice volume and sea level reconstructions. *Earth-Science Reviews*, *177*, 291–302. https://doi.org/10.1016/j.earscirev.2017.11.022

Regenberg, M., Nürnberg, D., Schönfeld, J., & Reichart, G.-J. (2007). Early diagenetic overprint in Caribbean sediment cores and its effect on the geochemical composition of planktonic foraminifera. *Biogeosciences*, *4*(6), 957–973. https://doi.org/10.5194/bg-4-957-2007

Reuning, L., Reijmer, J. J. G., Betzler, C., Swart, P., & Bauch, T. (2005). The use of paleoceanographic proxies in carbonate periplatform settings—Opportunities and pitfalls. *Sedimentary Geology*, *175*(1), 131–152. https://doi.org/10.1016/j.sedgeo.2004.12.026

Richey, J. N., & Tierney, J. E. (2016). GDGT and alkenone flux in the northern Gulf of Mexico: Implications for the TEX86 and UK'37 paleothermometers. *Paleoceanography*, *31*(12), 1547–1561. https://doi.org/10.1002/2016pa003032

Rippert, N., Nürnberg, D., Raddatz, J., Maier, E., Hathorne, E., Bijma, J., & Tiedemann, R. (2016). Constraining foraminiferal calcification depths in the western Pacific warm pool. *Marine Micropaleontology*, *128*, 14–27. https://doi.org/10.1016/j.marmicro.2016.08.004

Rohling, E. J., Foster, G. L., Grant, K. M., Marino, G., Roberts, A. P., Tamisiea, M. E., & Williams, F. (2014). Sea-level and deep-sea-temperature variability over the past 5.3 million years. *Nature*, *508*(7497), 477–482. https://doi.org/10.1038/nature13230

Rosenthal, Y., Holbourn, A. E., & Kulhanek, D. K. (2018). The Expedition 363 scientists. *Proceedings of the International Ocean Discovery Program*, 363. TX (International Ocean Discovery Program).

Rosenthal, Y., Lohmann, G., Lohmann, K., & Sherrell, R. (2000). Incorporation and preservation of Mg in Globigerinoides sacculifer: Implications for reconstructing the temperature and $^{18}O/^{16}O$ of seawater. *Paleoceanography*, *15*(1), 135–145. https://doi.org/10.1029/1999PA000415

Rosenthal, Y., & Lohmann, G. P. (2002). Accurate estimation of sea surface temperatures using dissolution-corrected calibrations for Mg/Ca paleothermometry. *Paleoceanography*, *17*(3), 16–11. https://doi.org/10.1029/2001pa000749

Rugenstein, M. A. A., Caldeira, K., & Knutti, R. (2016). Dependence of global radiative feedbacks on evolving patterns of surface heat fluxes. *Geophysical Research Letters*, *43*(18), 9877–9885. https://doi.org/10.1002/2016gl070907

Sadekov, A. Y., Eggins, S. M., Klinkhammer, G. P., & Rosenthal, Y. (2010). Effects of seafloor and laboratory dissolution on the Mg/Ca composition of Globigerinoides sacculifer and Orbulina universa tests — A laser ablation ICPMS microanalysis perspective. *Earth and Planetary Science Letters*, *292*(3–4), 312–324. https://doi.org/10.1016/j.epsl.2010.01.039

Samakinwa, E., Stepanek, C., & Lohmann, G. (2020). Sensitivity of mid-Pliocene climate to changes in orbital forcing, and PlioMIP's boundary conditions. *Climate of the Past Discussions*, *2020*, 1–35. https://doi.org/10.5194/cp-2020-5

Schauble, E. A., Ghosh, P., & Eiler, J. M. (2006). Preferential formation of $^{13}C–^{18}O$ bonds in carbonate minerals, estimated using first-principles lattice dynamics. *Geochimica et Cosmochimica Acta*, *70*(10), 2510–2529. https://doi.org/10.1016/j.gca.2006.02.011

Schauer, A. J., Kelson, J., Saenger, C., & Huntington, K. W. (2016). Choice of (17) O correction affects clumped isotope (Delta47) values of CO_2 measured with mass spectrometry. *Rapid Communications in Mass Spectrometry*, *30*(24), 2607–2616. https://doi.org/10.1002/rcm.7743

Schiebel, R., & Hemleben, C. (2017). *Planktic foraminifers in the modern ocean*. Springer.

Schlitzer, R. (2018). Ocean data view. Retrieved from http://odv.awi.de

Schmidt, D. N., Caromel, A. G. M., Seki, O., Rae, J. W. B., & Renaud, S. (2016). Morphological response of planktic foraminifers to habitat modifications associated with the emergence of the Isthmus of Panama. *Marine Micropaleontology*, *128*, 28–38. https://doi.org/10.1016/j.marmicro.2016.08.003

Schmid, T. W., & Bernasconi, S. M. (2010). An automated method for 'clumped-isotope' measurements on small carbonate samples. *Rapid Communications in Mass Spectrometry*, *24*(14), 1955–1963. https://doi.org/10.1002/rcm.4598

Schmuker, B., & Schiebel, R. (2002). Planktic foraminifers and hydrography of the eastern and northern Caribbean Sea. *Marine Micropaleontology*, *46*(3–4), 387–403. https://doi.org/10.1016/S0377-8398(02)00082-8

Schouten, S., Hopmans, E. C., & Damsté, J. S. S. (2013). The organic geochemistry of glycerol dialkyl glycerol tetraether lipids: A review. *Organic Geochemistry*, *54*, 19–61. https://doi.org/10.1016/j.orggeochem.2012.09.006

Schrag, D. P., DePaolo, D. J., & Richter, F. M. (1995). Reconstructing past sea surface temperatures: Correcting for diagenesis of bulk marine carbonate. *Geochimica et Cosmochimica Acta*, *59*(11), 2265–2278. https://doi.org/10.1016/0016-7037(95)00105-9

Seki, O, Schmidt, D. N., Schouten, S., Hopmans, E. C, Damsté, J. S. S, & Pancost, R. D. (2012). Paleoceanographic changes in the Eastern Equatorial Pacific over the last 10 Myr. *Paleoceanography*, *27*(3). https://doi.org/10.1029/2011pa002158

Spezzaferri, S., Kucera, M., Pearson, P. N., Wade, B. S., Rappo, S., Poole, C. R., et al. (2015). Fossil and genetic evidence for the polyphyletic nature of the planktonic foraminifera "Globigerinoides", and description of the new genus Trilobatus. *PLoS One*, *10*, e0128108. https://doi.org/10.1371/journal.pone.0128108

Stanley, S. M., & Hardie, L. A. (1998). Secular oscillations in the carbonate mineralogy of reef-building and sediment-producing organisms driven by tectonically forced shifts in seawater chemistry. *Palaeogeography, Palaeoclimatology, Palaeoecology*, *144*(1–2), 3–19. https://doi.org/10.1016/S0031-0182(98)00109-6

Stolper, D. A., Eiler, J. M., & Higgins, J. A. (2018). Modeling the effects of diagenesis on carbonate clumped-isotope values in deep- and shallow-water settings. *Geochimica et Cosmochimica Acta*, *227*, 264–291. https://doi.org/10.1016/j.gca.2018.01.037

Tierney, J. E., Haywood, A. M., Feng, R., Bhattacharya, T., & Otto-Bliesner, B. L. (2019). Pliocene Warmth Consistent With Greenhouse Gas Forcing. *Geophysical Research Letters*, *46*(15), 9136–9144. https://doi.org/10.1029/2019gl083802

Tierney, J. E., Malevich, S. B., Gray, W., Vetter, L., & Thirumalai, K. (2019). Bayesian calibration of the Mg/Ca paleothermometer in planktic foraminifera. *Paleoceanography and Paleoclimatology*. https://doi.org/10.1029/2019pa003744

Tierney, J. E, & Tingley, M. P. (2015). A TEX86 surface sediment database and extended Bayesian calibration. *Scientific Data*, *2*(1). https://doi.org/10.1038/sdata.2015.29

Tierney, J. E., & Tingley, M. P. (2018). BAYSPLINE: A new calibration for the alkenone paleothermometer. *Paleoceanography and Paleoclimatology*, *33*(3), 281–301. https://doi.org/10.1002/2017pa003201

Tripati, A. K., Eagle, R. A., Thiagarajan, N., Gagnon, A. C., Bauch, H., Halloran, P. R., & Eiler, J. M. (2010). ^{13}C–^{18}O isotope signatures and 'clumped isotope' thermometry in foraminifera and coccoliths. *Geochimica et Cosmochimica Acta*, *74*(20), 5697–5717. https://doi.org/10.1016/j.gca.2010.07.006

Wara, M. W., Ravelo, A. C., & Delaney, M. L. (2005). Permanent El Nino-like conditions during the Pliocene warm period. *Science*, *309*(5735), 758–761. https://doi.org/10.1126/science.1112596

White, S. M., & Ravelo, A. C. (2020). The benthic B/Ca record at Site 806: New constraints on the temperature of the West Pacific warm pool and the "El Padre" state in the Pliocene. *Paleoceanography and Paleoclimatology*, *35*(10), e2019PA003812. https://doi.org/10.1029/2019PA003812

Wit, J. C., de Nooijer, L. J., Haig, J., Jorissen, F. J., Thomas, E., & Reichart, G. J. (2017). Towards reconstructing ancient seawater Mg/Ca by combining porcelaneous and hyaline foraminiferal Mg/Ca-temperature calibrations. *Geochimica et Cosmochimica Acta*, *211*, 341–354. https://doi.org/10.1016/j.gca.2017.05.036

Wycech, J. B., Gill, E., Rajagopalan, B., Marchitto, T. M., & Molnar, P. H. (2020). Multiproxy reduced-dimension reconstruction of Pliocene Equatorial Pacific Sea surface temperatures. *Paleoceanography and Paleoclimatology*, *35*(1). https://doi.org/10.1029/2019pa003685

Zhang, Y. G., & Liu, X. (2018). Export depth of the TEX86 signal. *Paleoceanography and Paleoclimatology*, *33*, 666–671. https://doi.org/10.1029/2018pa003337

Zhang, Y. G., Pagani, M., & Liu, Z. (2014). A 12-million-year temperature history of the tropical Pacific Ocean. *Science*, *344*(6179), 84–87. https://doi.org/10.1126/science.1246172